SCHOOL OF MECHANICAL ENGINEERING – UNIVERSITY OF KWAZULU NATAL

ANALYSIS OF RESIDUAL STRESSES AND DISTORTIONS RESULTING FROM MULTI-PASS WELDING OF NOZZLES TO CYLINDRICAL PRESSURE VESSELS

In fulfillment of the MSc-Eng. Degree in Mechanical Engineering

Mthobisi Zondi - 210556841

1/9/2012

Supervisor: Professor Sarp Adali

DECLARATION

I, **Mthobisi Clyde Zondi** declare that:

(i) The research reported in this dissertation/thesis, except where otherwise indicated, is my original work.
(ii) This dissertation/thesis has not been submitted for any degree or examination at any other university.
(iii) This dissertation/thesis does not contain other persons' data, pictures, graphs or other information, unless specifically acknowledged as being sourced from other persons.
(iv) This dissertation/thesis does not contain other persons' writing, unless specifically acknowledged as being sourced from other researchers. Where other written sources have been quoted, then:
a) their words have been re-written but the general information attributed to them has been referenced;
b) where their exact words have been used, their writing has been placed inside quotation marks, and referenced.
(v) Where I have reproduced a publication of which I am an author, co-author or editor, I have indicated in detail which part of the publication was actually written by myself alone and have fully referenced such publications.
(vi) This dissertation/thesis does not contain text, graphics or tables copied and pasted from the Internet, unless specifically acknowledged, and the source being detailed in the dissertation/thesis and in the References sections.

Signed:……..

Date:……..

Place:……..

SUPERVISOR'S CONSENT

As the candidate's Supervisor I agree/do not agree to the submission of this thesis:

Professor Sarp Adali

Signed:…….

Date:……....

Place:……

ACKNOWLEDGEMENTS

The past 18 months have been long and exhausting in one way, and challenging and exciting in another. I would not have made it if it were not for the people that stood by me and rendered the much needed support.

I extend sincere gratitude to my Supervisor Professor Sarp Adali, whose guidance and assistance got me to eventually finish this dissertation within the targeted timelines. Mr. Strini Govender from the mechanical engineering workshop at UKZN Howard College was extremely helpful in organising the preparation of the weld-pieces at short notice, thank you Sir. I am very grateful to Mr Clint Bemont for his assistance with the experimental measurements, and for taking the time to guide me through the process.

I also acknowledge Mr Riaan Bergh, Manager: Testing Service at CSIR in Johannesburg for his assistance and guidance. Thank you. I am very grateful to Mr Greg Mitchell from Finite Element Analysis Services [FEAS] in Cape Town for taking the time to assist me get up to speed with the ABAQUS software. All my friends who took time off their busy schedule to commute with me between Durban and Johannesburg, I thank you. A big 'thank you' to my little brother Njabulo for his unwavering support, even when he did not understand what I was doing.

My lovely wife for her understanding and patience as I took away time that was budgeted for family events, thank you kindly my dear. The LORD is my Shepherd, I shall not want. Thank you God for the strength, the gift of mental capacity to get through this, and Your everlasting graciousness over me. Amen.

ABSTRACT

The purpose of the present study is to obtain insight into the formation, behaviour and magnitude of welding-induced residual stresses and distortions resulting from welding nozzles onto cylindrical pressure vessels. A hybrid methodology that comprises numerical analysis, experimental measurements and empirical calculations is used in the present study. The welding process induces a high thermal gradient on the material due to non-uniform temperature distribution; thereby causing the portion of the material that is exposed to high temperatures to expand. However, the relatively cooler material portion that is away from the weld pool resists such expansion, thereby subjecting the structure to stresses and distortions around the fusion zone (FZ) and the heat-affected zone (HAZ).

Over the last two decades a number of studies have been done in an effort to predict the effect of welding-induced residual stresses on the integrity of welded structures. However, to this end, such studies have focussed on analysing residual stresses on bead-on-plate, plate-to-plate and [to a less extent] on pipe-to-pipe weld joints. Fewer studies have looked at nozzle-cylinder joints of pressure vessels as is the case in this study. The second chapter gives a detailed review of applicable literature. The constitutive model described in the third chapter includes a two-phase sequentially-coupled thermo-mechanical analysis, which incorporates metallurgical effects. The non-linear transient problem is solved using an axisymmetric 2D model with 'element birth' technique, developed on ABAQUS. The first phase comprises the thermal analysis based on Goldak's moving heat source model that is used to determine temperature histories. The second phase is a sequel stress/strain analysis wherein the temperature fields are used as input loads.

The results discussed in chapters three and four show that there is a high concentration of residual stresses close to the weld centre-line, and these die down as distance away from centre-line increases. It is also shown that the inside surface is under tensile stresses, while the outer surface is under compressive stress, whose magnitude approaches yield strength of the material. Axial deflections of up to 0.384mm and radial shrinkage of 0.0237mm are observed. Distortion decreases as distance away from weld centre-line increases. Minimum axial shrinkage, which is close to zero, is observed at the restrained end. The analytical results show adequate corroboration and agreement with the experimental measurements. A number of mitigation techniques are suggested in order to alleviate the impact of residual stress and distortions on fatigue performance of welded structures.

Contents

LIST OF FIGURES

LIST OF TABLES

LIST OF ACRONYMS

ASTM	-	AMERICAN Society for Testing and Materials
bcc	-	body-centred cubic
CCT	-	Continuous Cooling Temperature
CG HAZ	-	Coarse Grain Heat Affected Zone
DC	-	Direct Current
fcc	-	face-centred cubic
FEA	-	Finite Element Analysis
FEM	-	Finite Element Method
FG HAZ	-	Fine Grain Heat Affected Zone
FM	-	Filler Metal
FZ	-	Fusion Zone
HAZ	-	Heat Affected Zone
HIC	-	Hydrogen-induced Cracking
HSLA	-	High Strength Low Alloy
JMAK	-	John-Mehl-Avrami-Kolmogorov
LBW	-	Laser Beam Welding
LOM	-	Light Optical Microscopy
MSR	-	Mechanical Stress Relief
PM	-	Parent Metal
PWHT	-	Post Weld Heat Treatment
SMAW	-	Shielded Metal Arc Welding
TSR	-	Thermal Stress Relief
TTT	-	Temperature Time Transformation

Chapter 1

Introduction

Pressure vessels comprise critical plant equipment within industrial operations. The fact that the vessel operates under pressure, and normally operates at high temperatures, necessitates that care is taken to ensure safety of humans operating it and the environment within which it operates. It is important therefore to exercise diligence when designing, fabricating and / or repairing pressure vessels, as any level of deviation may lead to catastrophic consequences. This study examines the residual stress distribution and distortions in a pressure vessel weld fusion zone [FZ], Heat Affected Zone [HAZ] and surrounding areas, arising as a result of welding nozzles onto pressure vessels.

1.1. Layout of the Report

The first chapter of this dissertation provides the background information to development and behaviour of residual stresses and distortions, the different types of residual stresses and distortions, the requirements and scope of the study, the research questions, and the envisaged methodological approach. The second chapter presents the overview of related literature, with specific focus on their relevance to the present study. The third chapter gives an account of how the Finite Element [FE] Model is formulated using the ABAQUS code, and how the developed model is used to solve the sequentially coupled thermo-mechanical problem, which is examined in the present study. The fourth chapter discusses the empirical and experimental methods used to verify results from the Finite Element Analysis [FEA] model discussed in the preceding chapter. The discussion of the results of numerical, empirical and experimental analyses is given in the fifth chapter; and furthermore this chapter gives the conclusions and recommendations of the study.

1.2. What is Residual Stress?

The Residual Stress Organisation defines residual stresses as '*those stresses that exist within a body in the absence of external loading or thermal gradients*'. According to Sterjovski (2003) residual stresses are those that remain in a structure after the removal of any externally-induced

loading. There is number of reasons why residual stresses would develop in metal structures, and these include manufacturing processes such as rolling, forging, casting and welding. During the welding process, thermal strains that occur as a result of heating and cooling cycles of the weld metal and surrounding areas, are the main course of residual stresses.

Karlsson (2005) states that residual stresses are in a balanced state within the component or structure, such that some parts of the structure experiences compressive stresses while others are under tensile stress. The maximum value that tensile residual stresses can attain is equal to yield stress of the material. Residual stresses may be beneficial or harmful to the structure depending on their nature and magnitude. Compressive residual stresses have been shown to have favourable effects in that they increase fatigue strength and reduce stress corrosion cracking and brittle fracture, amongst others. For this reason the compressive stresses may be deliberately introduced after the manufacturing process through shot-peening, autofrettaging, etc. [Siddique, 2005].

Pilipenko (2001) also states that stresses experienced by the body can either be externally stimulated [i.e. macro stresses] or can exist internally within the body without influence of an external force [i.e. micro stresses]. Residual stresses fall under the category of micro stresses. Internal stresses are in a self-equilibrium state. This implies that, notwithstanding the stress distribution in the body, the stresses in any cross-section are balanced by the sum of forces and the sum of moments of the forces.

Sterjovski (2003) observes that residual stresses can be classified into two groups according to their causes. The first category is that of residual stresses produced by structural mismatch, e.g. materials of different lengths forcibly welded together. The second category belongs to those residual stresses produced as a result of non-linear distribution of non-elastic mechanical and thermal strains. The two types of residual stresses normally found in pressure vessels are autofrettage-induced and welding-induced residual stresses. Both these types of residual stress fall under the second category stipulated above. Appendix A below provides more detail on the classification of residual stresses.

1.2.1 Autofrettage-induced Residual Stress

The concept of autofrettaging of pressure vessels is well-captured in Lee and Koh (2002) where the authors explain that in thick-walled pressure vessels fatigue cracks usually originate from the internal vessel surface and quickly grow into a fully-fledged fracture. The reason for such behaviour is that a pressurised thick-walled vessel is exposed to the largest tensile hoop stresses at the inside surface. In order to prevent early failure of a pressure vessel due to such tensile hoop stress, an autofrettage process that produces favourable compressive hoop stresses at the

inside diameter is normally employed. The induced compressive stresses counteract the tensile stresses caused by the internal pressure, thereby increasing the elastic strength of the vessel [Lee and Koh, 2002]. The dichotomy of this however is that the force equilibrium in the pressure vessel ensures that tensile hoop stresses are produced close to the outer surface of the vessel. Therefore an optimal situation is where the favourable impact of compressive hoop stresses is maximised, while the unfavourable impact of tensile stresses is minimised.

Maleki *et al* (2010) states that hydraulic autofrettage is '*a process whereby a cylindrical or spherical pressure vessel is subjected to high internal pressure till its walls become partially plastic*'. The above process has an effect of improving the fatigue life of the vessel through the resultant hoop residual stress. Therefore the utility of the autofrettage process is to produce compressive hoop residual stress around the internal surface of the pressure vessel thereby increasing its fatigue life [Maleki *et al*, 2010]. Balasubramanian and Guha (2004) observes that there is a 'causal-link' relationship between defected welds and weld-related failures, which suggests that a number of failure-related disruptions can be attributed to fatigue on its own. Furthermore, fatigue often comes before the commencement of brittle failure. Fatigue life extension is therefore a useful phenomenon.

Koh (2000) uses the local strain approach to investigate the '*low-cycle fatigue life of the autofrettaged pressure vessel with radial holes subjected to cyclic internal pressure*'. Local stress and strain distribution near the hole is determined through the employment of the elastic-plastic finite element stress analysis model. It was established that autofrettaging up to 50% OS (overstrain) had an effect of extending the fatigue life of the pressure vessel with radial holes by up to 45%. However, autofrettaging by more than 50% OS had no significant effect on the vessel's fatigue life. The reason for such findings is attributed to the fact that the autofrettage process produced detrimental tensile residual stresses near the outside surface of the pressure vessel, and high stress concentration around the holes.

It therefore follows that whereas autofrettaging can be significantly beneficial in as far as extending fatigue life of a pressure vessel is concerned, it can also easily be unfavourable if applied in a sub-optimal fashion.

1.2.2 Welding-Induced Residual Stress

The arc welding process uses the 'Joule effect' [i.e. generation of heat by passing electrical current through a conductor] to produce the energy required to fuse the metal pieces together. The base and filler metal are melted and joined together through the formation of the weld liquid pool. Depending on the material, the surface temperature of the piece varies from 1,700K (1,430°C) to 2,500K (2,230°C). In the weld liquid pool, convective effects take place that

improve the transportation of heat; and once heat source is removed the metal solidifies [Anca *et al*, 2010].

The understanding of welding residual stress formation is given in a very comprehensible way in Pilipenko (2001). Pilipenko illustrates the causes of welding residual stress and deformation through considering the metallic body to be made of numerous small cubic elements. The attempt to weld such a metallic body will induce high temperatures on it. Supposing that the induced heating was experienced equally amongst all the elements would in turn result in such elements being exposed to the same rise in temperature and therefore same magnitude of expansion in all directions. Due to such isothermal changes and equi-expansion amongst all elements, there would be neither internal stresses nor deformations formed as a result of the heating process.

However, supposing that the heating was not uniform amongst the elements would mean that each element experiences expansion that is commensurate with the temperature rise it is exposed to. In such a case each element would expand differently to the other, both in magnitude and direction. At the same time, the continuous nature of the metallic body would result in one element restricting the free expansion of the other, resulting in stress build-up. Such state of affairs changes the geometry and internal stress state of the elements, and hence the entire body.

If, during the heating process all elements were stressed elastically [i.e. below yield point], then the body would return to its initial stress-free condition after cooling. However, if the elements were stressed plastically [i.e. above yield point], then after cooling, each element would change dimensions proportionally to the amount of plastic deformation it experienced. The resultant changes in the state of the elements' internal stress and geometrical dimensions become permanent. Hence residual stress and distortions are formed in the metallic body.

The formation of welding-induced stresses and distortions can also be understood through *incompatible strain theory*. Feng (2005) holds that the residual stress distribution and the amount of weld distortion depend on the final state of the plastic strain distributions and their compatibility in the joint. The welding-induced incompatible inelastic strains in the weldment during the weld thermal cycle comprises transient thermal strains, cumulative plastic strains, and final inherent shrinkage strains. During welding, the incompatible thermal strains, resulting from the non-linear temperature distributions, generate the mechanical strains, which lead to incremental plastic strains, that accumulate during the thermal cycle, in the weldment if yielding occurs. The cumulative plastic strains then interact with weldment stiffness and the joint rigidity upon completion of welding cycles. This leads to the final state of residual stress and distortion in the FZ and HAZ.

1.3. Welding-induced Distortions

Distortions are caused by the non-uniform temperature distributions during welding. Similar to the residual stresses, distortions can also either be longitudinal [i.e. parallel to the weld seam] or transversal [i.e. perpendicular to the weld seam]. Furthermore, other types of distortions include angular distortions, which occur in the "through-thickness" direction; bending distortion and buckling distortion, which is caused by instability on thin plates. Whereas welding residual stress is mostly localised within the neighbourhood of the fusion zone and HAZ, welding distortion occurs through the entire structure. This usually causes problems when assembling welded components into other structures due to dimensional changes.

1.4. Arc Welding

The American Welding Society [AWS] defines welding as a "*localised coalescence of materials or non-metals produced by either heating of the materials to a suitable temperature with or without the application of pressure, or by application of pressure alone, with or without the use of filler metal*" [Anca *et al*, 2010]. The term *arc welding* refers to a sizeable group of welding processes that join metals through using an electric arc. Such welding processes include Gas Metal Arc [GMAW], Flux Cored Arc [FCAW], Submerged Arc [SAW], Gas Tungsten Arc [GTAW] and Shielded Metal Arc [SMAW]. The joining process is achieved through maintaining the heat from the arc between the tip of the electrode and the work-piece. The heat ensures that the metals are melted and joined together through the use of a filler metal.

For the purposes of this study, the Shielded Metal Arc Welding [also known as Manual Metal Arc Welding] process is considered. Figure 1.1 below illustrates the SMAW process. SMAW is a process that generates an arc through a stick-like electrode with flux covering. It is often called 'stick welding'. The electrical connection is as shown in Figure 1.1(a), where an electrode is connected to one terminal of the power source and the work-piece is linked to the other terminal. As the weld is laid, the flux coating of the electrode evaporates and gives off vapours and a layer of slag forms on top of the deposited weld metal [Figure 1.1(b)]. The released protective gas forms a shielding cloud over the molten weld pool to avert influx of impurities. The slag protects the weld from atmospheric contamination or oxidation as it solidifies.

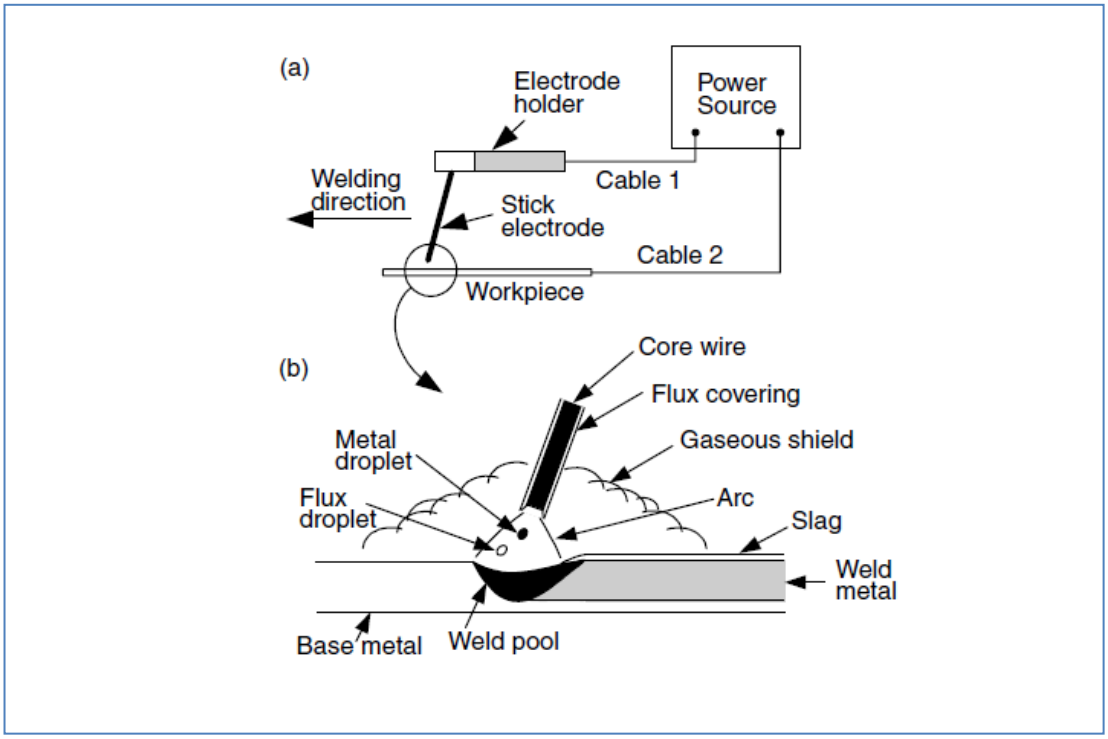

Figure 1.1. The Shielded Metal Arc Welding Process: (a) overall process; (b) welding area enlarged

Source: Kou (2003)

One advantage of the SMAW process is its simplicity, portability and inexpensiveness. On the other hand, the fact that the quality of the gas shield is lower compared to other arc welding processes [e.g. Gas-Tungten Arc Welding] works as a disadvantage, especially when welding oxidation-sensitive materials such as aluminium.

1.5. Welding Metallurgy

The resultant microstructure of the work-piece is significant for the determination of the mechanical properties and hence integrity of such work-piece once welded. The areas of the work-piece are the fusion zone [FZ], the heat-affected zone [HAZ], and the parent or base metal. Ideally the microstructure of all the three components should be the same, thereby ensuring the same properties across the work-piece; however in reality this is not the case. The final microstructure of the work-piece is affected by such parameters as cooling rate [i.e. cooling down rate from 800^{o}C to 500^{o}C or $\Delta t_{8\text{-}5}$], alloying additions, oxygen content and type of welding process. Continuous-cooling transformation [CCT] diagrams are usually used to explain the development of microstructure in carbon steels. CCT diagrams will be discussed in more in Chapter four below.

The HAZ region, being an intermediate location between the peak temperature-exposed weld metal and the relatively cool parent metal, experiences high temperature gradients during the welding process. Figure 1.2 below shows the various sub-regions of the HAZ in ferritic steels. Region 0 represents the unaffected base metal. Region 1 depicts the sub-region that was heated to below the lower critical temperature for austenitic transformation (A_1), whereas region 2 was heated to between A_1 and the upper critical temperature for complete austenite transformation (A_3). Region 2 contains a mixture of transformed austenite grains and the over-tempered parent metal [Zarzour, 1996].

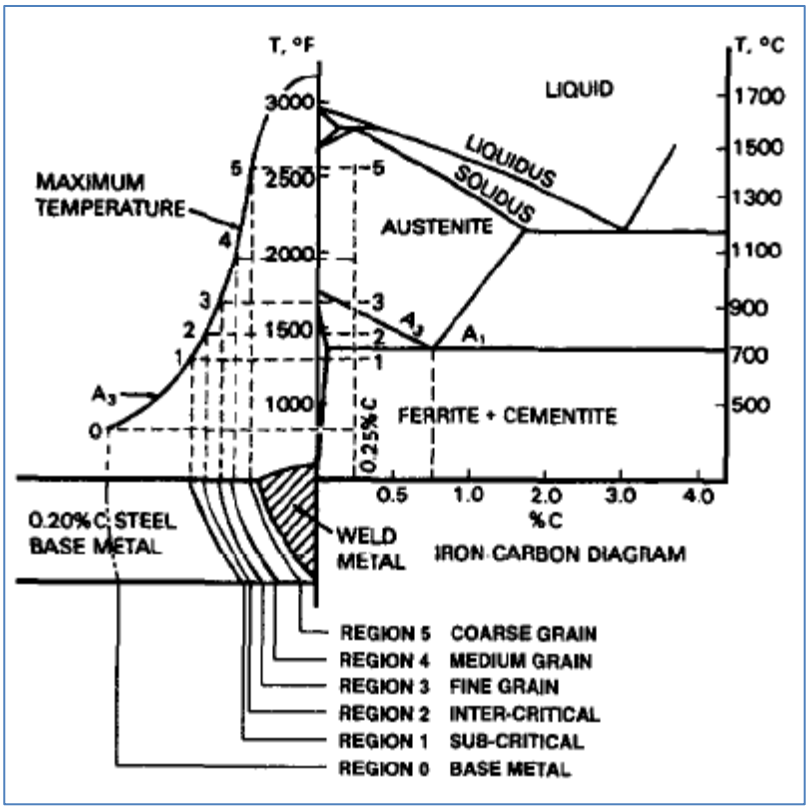

Figure 1.2. Relationship Between Various HAZ Sub-regions and Fe-C Phase Diagram

Source: Zarzour *et al* (1996)

Region 3 represents a complete austenite transformation with little or no grain growth. This region is known as fine grain HAZ or FG HAZ. Region 4 experienced some grain growth and homogenisation, whereas the coarse grain HAZ [CG HAZ] represented by region 5 was exposed to temperature close to melting, and underwent significant grain growth. In a multi-pass weld, region 5 is exposed to some grain refinement due to the reheating effect from subsequent weld-passes.

1.6. Research Questions

This study purports to answer the following questions:

a. **What does the residual stress distribution looks like in a multi-pass full-penetration weld of a nozzle onto a pressure vessel?**

   The magnitude and direction of the residual stresses within various positions of the weld-piece will be determined and plotted against the proximity to the weld zone in order to determine the potential impact to the integrity of the structure.

b. **What types of distortions or deformations arise as a result of welding nozzles onto cylindrical pressure vessels?**

   The magnitude and characterisation of welding-induced distortions and their significance in influencing the life expectancy of the welded pressure vessel structure will be examined.

c. **What is the final matrix microstructure of the weld region and the heat affected zone [HAZ], and how does this influence the integrity of the pressure vessel?**

   The proportions of martensite, bainite, ferrite and austenite that exist within the microstructure of the weld region and surrounding areas are to be evaluated in order to understand the metallurgical appearance of the structure, and hence to be able to predict its thermo-mechanical properties.

d. **What type of changes in mechanical properties of the weld region, HAZ and the parent metal does the welding process bring about?**

   The yield strength, toughness and hardness will be worked out before and after welding through experimental methods. This will give the change in mechanical properties introduced by the welding process, and the effect thereof.

e. **What are the main factors affecting welding-induced residual stresses and distortions in pressure vessel nozzle welding, and how can these be optimised in order to mitigate their impact?**

   Using available literature, investigations into which influential factors contribute substantially to the formation and behaviour of welding-induced residual stresses and distortions shall take place and answers to this question provided.

1.7. Research Methodology

Leggatt (2008) holds that "the best approach for reliable determination of residual stresses is by a combination of measurements and modelling. Any discrepancies should be investigated, and improved measurements and modelling methods should be applied until consistent results are obtained". The approach taken is this study is influenced by this assertion. A combination of numerical (finite element methods), empirical (formulae-based calculations) and experimental (lab testing) methods are used in this study. The detailed methodological approach is discussed in chapters three and four below.

1.8. Requirements and Scope of Present Study

Given the preceding discussion, it is clear that while welding is widely used in permanent processes for steel manufacturing and fabrication applications, there is still a number of adverse effects that such process inevitably causes. A number of studies and analytical evaluations have been done in an effort to predict the effect and influence of welding-induced residual stresses on the integrity and fatigue life of welded structures. However, to this end such studies have focused on analysing welding-induced residual stresses on bead-on-plate, plate-to-plate and (to a less extent) on pipe-to-pipe weld joints. There have been fewer studies that looked at nozzle-cylinder joints on pressure vessels.

In most industrial applications, pressure vessels have to have nozzles for operations purposes. These may range from small inert gas purge nozzles to large man-hole covered access nozzles. Given their weld joints and associated residual stresses, such nozzles present a level of vulnerability to the pressure vessel integrity that need to be understood in order for mitigation measures to be taken. It therefore follows that detailed analytical studies of welding-induced residual stresses and distortions on nozzle joints of pressure vessels stand to provide a host of benefits in design optimisation, reduced failure rate, improved fatigue life, reduction of environmental pollution and reduction in cost of re-welding or re-working of structures.

The aim of this study therefore is to investigate transient and residual welding stresses and distortions in multi-pass nozzle welds of pressure vessel structures, and to recommend mitigating measures for reducing their negative impact on life-expectancy and performance of the welded structure.The scope of work in this dissertation is limited to the circumferential welding on nozzles onto cylindrical pressure vessels made of high strength carbon steel. The present investigation focuses on the welding- induced residual stresses and distortions through applying a combination of finite element modelling, empirical calculation, and verification experiments.

The next chapter looks at the review of relevant literature with specific focus on its relatedness to the subject of this dissertation.

Chapter 2

Literature Review

Since the early 1970's a number of studies on welding process simulations ranging from heat source modelling to materials micro-structure investigations and other related aspects has been done. One of the initial (first) works on finite element method [FEM] application to stress/strain analysis produced a FE algorithmic procedure to numerically generate residual stress through a moving heat source simulating the welding process. This work was performed by Rybicki *et al* (1977). The authors employ a hybrid-type analysis that combines experimental and computational methods whereby simple FE techniques are used to incorporate the measured (through ultrasonic shear waves) residual stress during crack analysis. The study identifies the significance of the residual stress distribution ahead and behind the advancing crack tip in relation to plastic zone size in the area. Further earlier work on heat source models included models on multiple-point heat sources by Rybicki *et al* (1978). Ued and Yamakawa (1971) and Hibbitt and Marcal (1973) performed some of the early works in simulations of welding processes using the finite elements method. Friedman (1975), Rybicki *et al* (1978) and Andersson (1978) presented further work on simulation methodology through using sequentially coupled analysis technique.

Subsequent to the early work given above, there were numerous studies of welding process using finite elements method, and a corresponding number of experiments were made to validate the results from modelling techniques. Welding-induced residual stress has since received increasing attention within the welding research community in the last 20 years. Dong *et al* (2005) observe that the driving force behind such interest is that '*application of modern structural integrity assessment procedures for defective welded components requires more accurate information on the weld residual stress state to give a more realistic assessment*'. Furthermore, the need to better understand and characterise residual stresses associated to pressure vessel repairs has become more evident; especially since weld repairs have become a structural integrity concern for ageing pressure vessel and piping components. [Dong *et al*, 2005].

In their later study that sought to develop a residual stress prediction model on a multi-pass butt-welded 2.25Cr-1Mo Steel pipes, Deng and Mukarawa (2008) came up with thermal-metallurgical-thermal computational procedure based on an ABAQUS code. The authors found

that on the inside surface of the pipe, tensile residual stresses were produced near the weld fusion zone and the HAZ; while compressive residual stresses were generated away from the FZ and HAZ. The outside surface showed an opposite of the inside, with compressive stresses generated at the FZ, while relatively large tensile stresses were produced away from the FZ.

Brust *et al* (1997) summarise recent findings, which investigated the effect of residual stress fields on crack growth in pipes and cylindrical vessels, and conclude that crack growth behaviour observed in repair welds may be quite different to that of original fabrication welds.

2.1 Definitions used in Numerical Analysis *[Lindgren, 2006]*

For the purposes of this dissertation's context, and in particular the literature review discussed hereunder, the terms used herein will be defined as follows:

a. A model refers to a finite element model that is used to present certain aspects of the behaviour of the system.
b. Simulation is an imitation of the internal process, and not just the resultant outcome, of the system under investigation
c. Validation is the process where the accuracy of the model is evaluated by comparing model results with experimental results.
d. Calibration is the determination of parameters in order to create a match with some predetermined measurements
e. Verification is the process where it is assured that the model is correct with respect to the conceptual model
f. The conceptual model comprises the governing mathematical equations chosen to define the various aspects and parameters of the FE input file
g. Qualification is the process of assuring the integrity of the concept model with respect to reality

The discussion below attempts to group the research works according to their objectives and focus.

2.2. Factors that Influence Residual Stress

There is a number of factors that have an influence on welding-induced residual stress distributions in a weld-piece. Anca *et al* (2010) observe that a number of factors have influence on the magnitude of the residual stresses and their distribution, including the type of welding, number of passes, material properties and degree of constraint or restraint. They further conclude that material that is rigidly constrained will have greater residual stresses than one that is allowed to distort freely during the welding process. Leggatt (2008) resolves that residual

stress is affected by '*numerous factors, including the geometry of the parts to be joined, the use of fabrication aids such as tasks, cleats and jigs, the pass sequence for multi-pass welds and the welding sequence for structures with more than one weld*'. Furthermore, material properties, such as coefficient of thermal expansion, yield strength, and metallurgical phase change may also influence residual stresses.

2.2.1 Welding Restraints

The restraint at a weld joint may be described as the resistance to the free movement in any direction of the heated material [Leggatt, 2008]. Leggatt (2008) performs a study whose aim is to provide an overview of how the specified 'principal factors' affect the magnitude, direction and distribution of residual stress in welded joints and structures. Tests done show that residual stresses may be found at a distances considerably away from the weld, and do not always dies out rapidly between one or two plate thicknesses, as is usually claimed. The author established that restraints during welding, as well as materials used have significant impact on the magnitude and distribution of welding-induced distortions on structures.

2.2.2 Post Weld Heat Treatment and Residual Stress

Sterjovski *et al* (2004) in their analysis of cross-weld properties of quenched and tempered (QT) steels defines post weld heat treatment [PWHT] as '*a stress-relieving process whereby residual stresses are reduced by heating between 540 and 590^{o}C for a set time depending upon plate thickness*'. Their study concentrated on transportable pressure vessels. All residual stresses were found to be compressive, and the maximum value recorded through experiments was 205 MPa. Furthermore the authors discovered that whereas the weld metal hardness and base metal hardness were suitably matched before PWHT, the hardness of the weld metal decreased below that of the base metal after PWHT [Sterjovski et al, 2004].

Legatt's (2008) testing of residual stress in a circumferential weld of C-Mn Steel pipe before and after PHWT showed that PHWT has the effect of reducing residual stresses significantly in magnitude. Smith *et al* (1997) perform a study whose purpose is to '*provide detailed information on the effect of a long PHWT on the microstructure and mechanical properties of a welded joint in ASTM A302, Gr B Pressure Vessel Steel*'. They conclude that Post Weld Heat Treatment (PWHT) has an effect of reducing welding-process-induced residual stresses, while also tempering the Heat Affected Zone (HAZ). However, excessive PWHT may have undesired consequence such as reducing weld metal strength.

2.2.3 Effect of Welding Process

Moraitis and Labeas (2009) state that most welding processes operate in conduction limited mode such that the heat deposited onto the surface of the components being welded is conducted through the metallic material. In the Heat Affected Zone, and particularly the keyhole area, inter-related optical and physical phenomena, such as laser light absorption, reflection and phase change, are further observed.

Maraitis and Labeas (2009) develop a prediction model for residual stresses and distortions due to Laser Beam Welding (LBW) of butt joints in pressure vessels. The authors performed a two-level analysis; namely localised (level-1) three-dimensional model for keyhole attributes prediction, and a global (level-2) model. The level-1 model was developed by means of non-linear thermo-mechanical analysis, and is used to predict 'keyhole' shape and size. The global welding simulation model represented the entire welded configuration, and used results from level-1 simulation in order to compute residual stress and strain fields. The authors conclude that due to its inherent capabilities to focus in small spot diameter, through its high-power density welding technology, the Laser Beam Welding (LBW) process produces a narrower Heat Affected Zone (HAZ), resulting in less distortions, residual stresses and strains compared to conventional welding methods (e.g. TIG, Arc and Electric Beam Welding).

In their study to determine the effect of welding processes on toe-cracking behaviour of fillet-welds on a Pressure Vessel Grade Steel, Balasubramanian and Guha (2004) concluded that the welding process significantly influenced the crack initiation life of the joints failing from the toe region. The authors compared fatigue performances of cruciform joints fabricated by the semi-automatic Flux Cored Arc Welding (FCAW) and the manual Shielded Metal Arc Welding (SMAW). Fatigue crack growth was experimentally measured using Vertical Pulsar of 200kN capacity. It was established that fatigue growth rate is relatively less in SMAW joints than in FCAW joints. This is because crack initiation is delayed in SMAW joints, and hence crack initiation life is longer as compared to FCAW joints. Furthermore, it was found that the lower heat input of the SMAW process ensures that the Coarse Grain HAZ (CGHAZ) contains low carbon martensite, while the higher heat input in FCAW process causes formation of bainitic structure in the CGHAZ region. It therefore follows that whereas automatic welding process (e.g. Submerged Arc Welding) are normally favoured over their manual counterparts due to higher productivity, lower costs, and better control of geometry; it was noted however, that the service lives of such automatic welds are usually shorter than that of manual welds [Balasubramanian and Guha, 2004].

Teng and Chang (1998) observe that high-speed welding [e.g. Laser Beam Welding] yields a slightly narrower isotherm, thereby influencing the shrinkage of butt welds and reducing

residual stress. Furthermore, high welding speed reduces the amount of adjacent material affected by the heat of the welding arc. The magnitude of the HAZ is therefore relatively smaller.

2.2.4 Effect of Weld Conditions

In their analytical study of residual stresses in repair welds, Dong *et al* (2005) established that welding conditions (e.g. heat input, number of passes, and inter-pass temperature) are important parameters when analysing repair weld residual stresses. The temperature of the weld-piece before and during welding may have an influence on the residual stress distribution of such weld-piece. The preheat temperature is the one which the work-piece is heated to prior to welding. The inter-pass temperature is the temperature of the work-piece before each run is deposited in multi-pass applications. Keehan (2004) holds that both these parameters have a significant effect on the weld cooling rate, and hence the final microstructure.

Keehan (2004) also observes that the heat generated during the welding process is a function of current, voltage and welding speed. Increasing heat input increases the area of weld bead, and may result in fewer runs being required to completely fill up the weld. In a multi-run weld, high heat input removes most of the columnar structure, and improves toughness. The author further states that the diameter of the electrode is proportional to the heat input, and hence it increases cooling times. Furthermore, the larger electrode diameters increase the amount of columnar region in the weld metal, thereby decreasing the magnitude of re-austenitised and tempered areas within the weld. This in turn increases the weld metal hardness and reduces toughness.

Having studied weld joints in both 'as-welded' and after PWHT conditions, Smith *et al* (1997) conclude that the effect of high heat input welding on mechanical properties of the joint tend to be more significant at the HAZ than the weld-metal. The toughness of the HAZ therefore becomes the determining factor of the integrity of the weld joint produced by high weld heat input (i.e. 4.3 kJ), and not so much the weld metal. Furthermore, the width of the HAZ increases with increasing heat input.

Qureshi (2004) used a combination of experimental and numerical methods to determine impact of welding speed on residual stress. The study showed that for the lowest welding speed, residual stresses were in their highest magnitude for both internal surfaces [tensile stresses] and external surfaces [compressive stresses] of the cylinder. Lower welding speed results in higher heat input per unit length, and consequently wider FZ and HAZ. It has been demonstrated in many studies that varying heat input, with everything else remaining constant, will have an influence on temperature distributions and hence the residual stresses of a welded structure. In a

study performed by Qureshi (2004), it was shown that heat input increase causes a corresponding increase in residual stress.

Siddique (2005) establishes that increasing heat input per unit length has an effect of increasing the magnitude of residual stresses and their zone of influence. Malik *et al* (2007) solved a transient non-linear thermo-mechanical problem of a pipe-to-shell multi-pass butt weld joint using FE modelling and experimental validation. The authors established that welding speed, heat source parameters and total heat input significantly affect the resultant outlook of FZ and HAZ.

Gery *et al* (2005) provide a thermal simulation study of a plate butt joint using FE transient heat transfer analysis with the objective to determine energy input, impact of heat source distribution, and welding speed on resultant temperature distributions. Their study revealed that welding speed, heat source distributions, and energy input has significant impact on the shape and boundaries of the FZ and HAZ. The temperature distributions were also impacted, as well as the residual stresses and distortions.

2.2.5 Weld-piece Geometry

In their investigation of the effects of pipe geometry on residual stresses – especially the effects on circumferential variations of residual stresses – Lee and Chang (2008) established, through a 3D thermo-mechanical FE model, that the pipe diameter influences the axial and hoop residual stresses in thin-walled pipe welds. The authors conclude that the thinner walled pipes have lower tensile residual stresses compared to the thicker walled pipes. Dong (2003) concludes that pipe radius and thickness have an influence on residual stress. In their study to analyse the thermo-mechanical behaviour and evaluate the distributions of residual stresses in circular patch welds through finite element [FE] techniques, Teng *et al* (2000) discovered that the weld line experiences contractions after patch welding. The resultant circumferential residual stress is close to the material's yield strength. They further established that as the size of the patch decreases, the residual stress in the patch centre increases.

Siddique (2005) concludes that pipe diameter has significant effect on the magnitude of the residual stresses as well as on the zone of influence. The peak values of the axial residual stresses near the weld centreline and their zone of influence increase with pipe diameter. The author also concludes that increasing pipe wall thickness has an effect of decreasing the magnitude of residual stress. This can be attributed to the fact that a pipe of smaller wall thickness has low stiffness and is more prone to the radial shrinkage resulting from bending stresses. It was however noted that the zone of residual stresses increases with pipe wall thickness. Qureshi (2004) established that for both circumferential and axial welds residual

stress varied proportionally with the diameter of a cylinder. This is accredited to increased cylinder bending for larger diameters. The author further worked out that the larger wall thicknesses reduced residual stress, and increased the stress zone. Qureshi also studied the impact of root-gap opening and established that axial stress profiles showed no significant variation against changes in root-gap, while tensile hoop stress was slightly higher for zero root-gap.

2.2.6 Mechanical Properties

Anca *et al* (2010) hold that the most important mechanical properties during residual stress evaluation are Young's modulus, thermal dilatation coefficient, and (to a lesser extent) Poisson's ratio. According to Deng and Murakawa (2008) the two main factors that generally affect welding residual stresses are shape deformation, i.e. strain, and the variation of mechanical properties such as yield strength

Nonaka *et al* (2001) evaluate performance of repair welds applied to degraded materials of high temperature and high pressure system. They performed a number of mechanical properties tests on the base metal, weld fusion zone and the HAZ, including hardness tests, creep tests, Charpy impact test and creep-fatigue tests. They established that the Charpy impact energy of the simulated HAZ materials, of header base material and of the girth welded materials were much higher than those of the base metal. This suggested that heat conducted during the repair welding restored the ductility of these materials. Deng and Murakawa (2008) conclude that hoop residual stress on the outside surface is influenced by Yield Strength during phase transformation process.

Karlsson (2005) attempts to estimate residual stresses that arise as a result of welding nozzles onto a pressure vessel. The author establishes that whereas the circumferential residual stress tends to depend on the yield strength of the material, irrespective of the geometry of the weld-piece, the radial residual stress varies disproportionately with the pipe radius, i.e. the smaller the pipe radius, the higher the radial residual stress. The maximum value of radial residual stresses for the materials studied ranges between 60 and 80% of the yield strength.

2.2.7 Welding Sequence

Teng *et al* (2003) perform a thermal elasto-plastic analysis using finite element techniques to analyse the thermo-mechanical behaviour in circular patch welded plates. Their study includes single pass and multi-pass butt welds. The sequences that were examined were back-step welding, progressive welding and jump welding. The authors establish that '*a large tensile stress occurs near the weld bead and a comprehensive stress appears away from the weld bead*

in longitudinal residual stresses along the X-direction for single-pass and multi-pass butt welds'. In this study the authors recommend back-step welding as a preferred welding sequence for circular patch welds. This sequence has a relatively more favourable effect to residual stress compared to progressive welding and jump welding sequences. This can be attributed to the 'heat-treatment effect' on the tail of the preceding weld run. The discussed welding sequences are shown in figure 2.1 below.

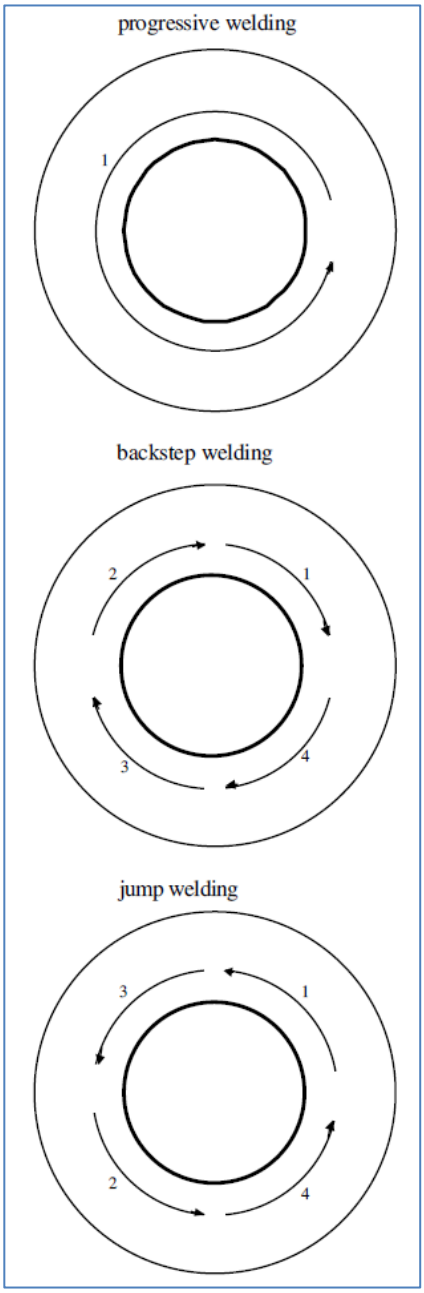

Figure 2.1: Various Welding Sequences for Circumferential welds

Source: Teng *et al* (2003)

Teng *et al* (2003) also advise that in order to prevent the rigid restraint in the weld bead, and thereby consequently decreasing residual stress, more free space should be made available for free movement of the welding structure during the welding procedure. Sattari-Far and Javadi (2008) present a '*parametric study to determine the effect of welding sequence on welding distortions of pipes*'. The authors employ a sequentially-coupled 3D thermo-mechanical analysis to study nine various welding sequences and their impact on resultant distortions. It was established that a continuous segment as well as tail-joining segments of the weld bead resulted in higher welding induced distortions than an alternating segment sequence, which ensures that weld metal is deposited evenly across the circumference of a pipe in a progressive fashion.

Ozcatalbas and Vural (2009) investigate the impact of various welding sequences on distortion tendencies in welding of steel lattice beams through the use of distortion forces. The employed experimental methodology comprises the use of force measuring plates to measure distortion forces created by welding cycle on the beam. Twenty different welding sequences were evaluated, and minimum distortion was observed while using a welding sequence of mixed type, and which is based at the end of the beam. Gannon *et al* (2010) determine the influence of welding sequence on residual stress and distortions in flat bar stiffeners applicable in ship hull construction. The authors use a sequentially-coupled thermo-mechanical elasto-plastic model to evaluate four different welding sequences. Similar to the previous studies, it was also established that the welding sequence that employed an alternating segment method – in both location and direction – produced the least residual stress and distortions compared to other welding sequences.

2.2.8 Metallurgical Phase Transformation

Lee and Chang (2009) determine residual stresses in a multi-pass butt-welded high-strength steel plate through employing a sequentially-coupled 3D thermo-metallo-mechanical FE analysis, incorporating metallurgical effects. The developed FE model incorporates volumetric change and variation in yield stress of the base metal and weld metal due to martensitic and austenitic transformations. The authors establish that volumetric increase during the austenitic-martensitic transformation [i.e. during cooling] has an effect of reducing longitudinal tensile residual stresses in the weld region and the HAZ.

Deng and Murakawa (2006) analyse thermal effects, phase transformation effects and mechanical effects in multi-pass butt-welded steel pipes. Using a thermal elastic-plastic finite element model they conclude that the volumetric change as a result of martensitic transformation has a significant influence on welding residual stress. The effect results in

change of both the magnitude and direction of residual stress in the weldment. They further state that the Yield Strength change induced by solid-state phase transformation is also influential to the resultant welding-induced residual stress.

Yaghi and Becker (2004) explains that '*strains are induced when solid phase transformation from austenite to ferrite, pearlite, bainite and martensite take place during cooling, caused by local material dilatations*'. Such dilatations are assumed to be proportional to the fractional quantities of the transformed material phases, which in turn are iteratively determined for each time step in the thermal analysis. Leggatt (2008) observes that phase change is yet another material property factor that affects residual stresses. In particular, the temperatures at which the phase transformation commences and terminates are sensitive to the cooling rate. Where the cooling rate is fast, e.g. HAZ, phase transformation occurs at relatively low temperatures.

Deng and Murakawa (2008) study incorporated solid-phase transformation effects. They established that '*the final matrix microstructure of the weld zone and the HAZ is a mixture consisting of bainite and martensite, with the volume fraction of bainite being higher than that of martensite*'. Their simulation results demonstrated that in order to obtain precise prediction results, phase-dependant material properties such as yield strength were needed. Deng (2009) holds that previous experimental studies have shown that measured stresses in the fusion zone [FZ] and HAZ are lower than those in the base metal adjacent to the HAZ. This is because of the volumetric change of the material due to martensitic transformation in a relatively low temperature. The author concludes that martensitic transformation has significance influence on the welding residual stress for med-carbon steels.

It has been shown in previous studies that when analyzing welding-induced residual stresses on high strength carbon steels solid-state phase transformation should be taken into account in the welding simulation, given that it induces important physical and mechanical effects such as volumetric changes in the material [Lee and Chang, 2009].

When steel is heated above the 'A_1' temperature, its structure starts to transform from body-centred cubic (ferritic) structure to face centred cubic (austenitic) structure. During cooling the austenite changes back to martensite, whose micro-structure will depend on how rapid the cooling is [Deng and Murakawa, 2006]. The diagrammatical illustration of this behaviour is shown in figure 2.2 below. The solid-state phase transformation represented in figure 2.2 below is due to thermal cycles that take place during the welding process. When pearlite-ferrite carbon steel is heated over 'A_1' temperature during the heating phase of welding, its microstructure starts to transform into austenite, and when the temperature reaches 'A_3' pearlite-ferrite completely changes to austenite. The volume change due to this martensitic transformation is

represented in figure 2.2 below. The quantity of martensite formed depends on the temperature reached during cooling [Lee and Chang, 2009].

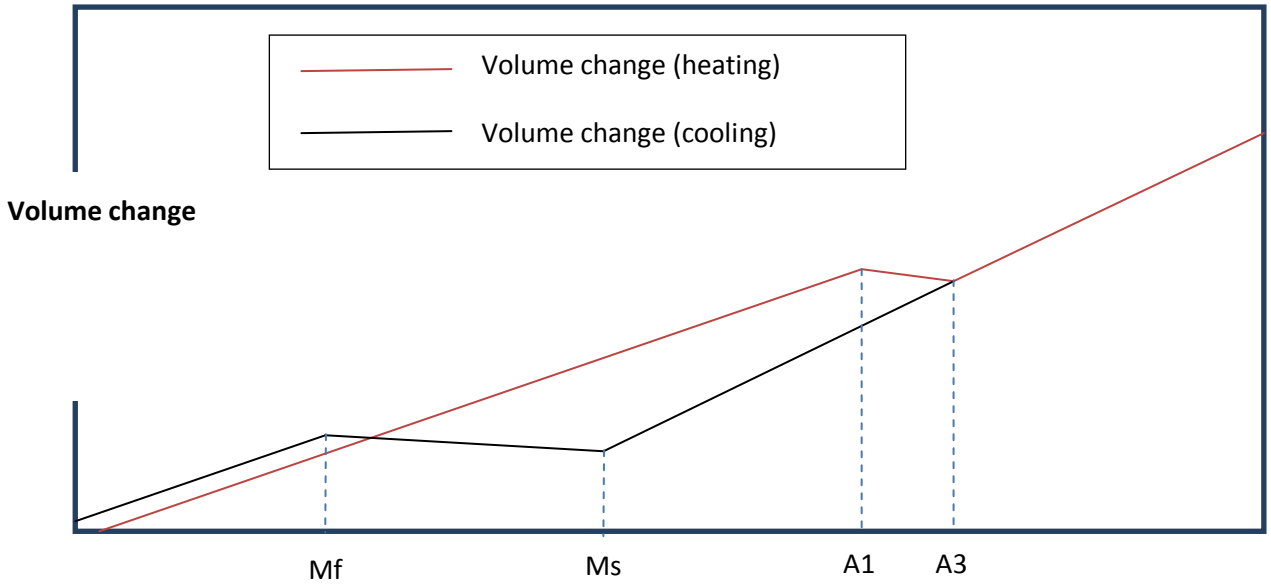

Figure 2.2: Volume Change due to Phase Transformation

Source: Lee and Chang (2009)

Pilipenko (2001) observes that microstructural transformation at low temperatures [i.e. martensitic] in the fusion zone and the HAZ can change the residual stress distribution significantly; whereas transformations achieved at high temperatures [i.e. austenitic] may have no significant impact on residual stress distribution.

2.3. Three-Dimensional (3D) versus Two-Dimensional (2D) FE Models

When comparing 2D and 3D modelling, Siddique (2005) concludes that "through proper modelling of the welding arc, almost identical transient temperature distributions can be achieved in both the two and three dimensional models for the same arc parameters". The author further states that while comparing residual stress distributions from 2D and 3D models, it was clear that the two results were adequately comparable for engineering judgements purposes.

In their study to evaluate temperature fields and residual stress in multi-pass welds of stainless steel pipes through a finite element procedure developed in the ABAQUS code, Deng and Murakawa (2006b) established that results from 2D and 3D simulations showed very good

correlation between the two models. They then conclude that a 2D model can therefore accurately predict the thermal cycles during steel pipe welding.

Chapter 3

Numerical Analysis

Finite Element Analysis [FEA] is a numerical modelling scheme utilised for simulation of engineering structures in order to virtually study the expected behaviour of such structure under particular conditions. The significance of this method is the capability to isolate essential parameters of the complex welding process and procedure to study the effects of respective parameters on the formation of welding-induced stresses and deformation. Although experimental methods are used to calibrate the simulation procedures, the latter still however has an advantage that they can be used for systematic investigations on relevant parameters which may not be accommodated by experimental studies alone [Feng, 2005].

Kisioglu (2005) observes that while many researchers have developed analytical and experimental methods to predict the effect of weld joints on structural behaviour; advances in computer-aided modelling such as FEM have helped even further the analysis of structural behaviour in welded components. The complexity of the welding simulation problem can be appreciated through considering that the enormous temperature differential in the arc area creates a non-uniform distribution of heat in the work-piece. The increasing temperature causes: a decrease in yield strength, an increase of the coefficient of thermal expansion, a decrease in thermal conductivity, and an increase in specific heat. Furthermore, welding causes changes in the physical and metallurgical structures in the weld [Feng, 2005]. The process of determining the welding stresses and distortions through FEA simulation is therefore an inherently difficult problem to solve.

3.1 Modelling Approach

3D numerical modelling is accepted as an effective method of solving complex welding problems accurately. However the computing time and costs make this method unviable for practical industrial applications. Alternatively, 2D modelling or a hybrid model of 2D and 3D elements is accepted as a realistic alternative modelling approach for practical applications. The main features of the FEA Model are discussed below.

Taylor *et al* (2002) stipulates two alternative ways in which numerical simulation of the welding process can take place, namely the *thermo-fluid* approach and the *thermo-mechanical* approach. In the thermo-fluid approach, the complex fluid and thermo-dynamics local to the

weld pool are modelled by observing the weld pool and the HAZ. The physical characteristics of the molten weld pool as well as the HAZ are represented through the conservation of mass, momentum and heat equations, together with the surface tension and latent heat boundary conditions. Alternatively, the thermo-mechanical behaviour of the weld structure could be modelled, with specific focus to the heat source. A variety of heat source models can be used in the simulation of welding, whose accuracy relies on the empirical and theoretical parameters describing the weld pool shape and size [Yaghi and Becker, 2004]. A thermo-mechanical modelling approach, incorporating a 2D model, is adopted in this study.

3.2 Geometrical Modelling Strategy

There are three general types of FEA models that are usually applied for welding stress prediction [Feng, 2005].

a. *Axisymmetric model*. When both geometry and loading have a common axis of symmetry, the axisymmetric condition exists.
b. *Plane-stress model*. This condition exists when the plate thickness is small or the temperature and stress changes in the thickness direction are negligible. Mostly used in 3D structural analysis
c. *Generalised plane-strain model*. It assumes the existence of a plane, which contains all displacement vectors that have a constant strain value normal to the plane [i.e. a cross-sectional plane remains a plane when it deforms]. For 2D modelling analysis of a weld cross-section, the generalised plane-strain condition must be specified in lieu of the general plane-strain condition that restricts displacements normal to the cross-sectional plane. This condition assumes complete rigidity of the cross-section such that the entire cross-section yields under load.

3.3 The Thermo-metallo-mechanical [TMM] Problem

In order to understand the thermodynamic and physical interaction phenomenon that occurs during welding, it is important to understand the individual aspects involved in this non-linear interactive relationship. Figure 3.1 below represent the schematic features of this phenomenon. During welding, the non-uniform temperature distribution experienced by the material causes thermal stress(1), and the induced phase transformation (2) affects the structural distribution in the solid-liquid transition or martensitic / pearlitic transformations in the solid phase. This brings about transformation stress (3), and interrupts the strain field in the body. According to Feng (2005), arrows in the opposite direction indicate interaction in the following manner. Existing stress in material performs work, some of which is converted into heat (4), thereby affecting the temperature distribution. Stress-strain aspect has an effect of accelerating phase

transformation (5). There is also latent heat released due to phase transformation (6), which affects the temperature distribution.

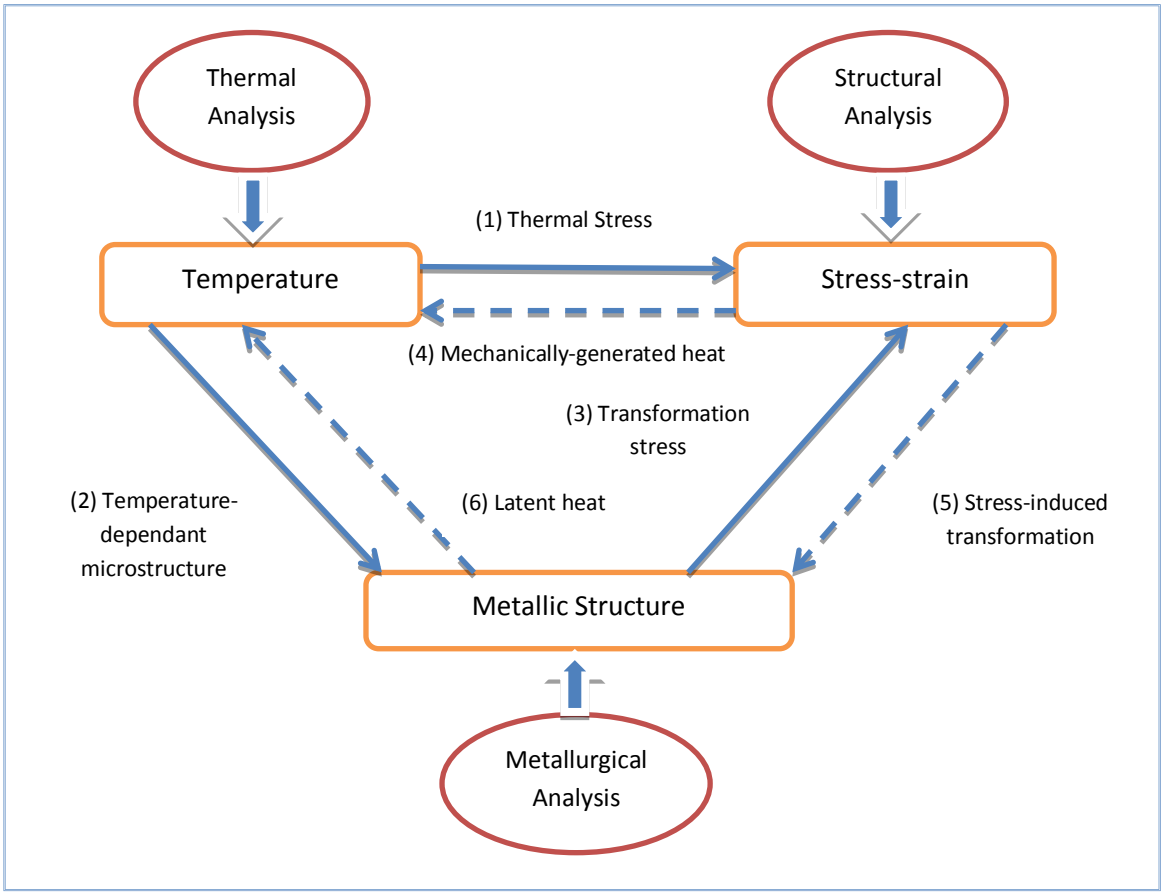

Figure 3.1: Thermo-metallo-mechanical Interaction During Welding

Source: Feng (2005)

In this study, a non-linear time-dependant thermal elastic-plastic analysis of a moving heat source is performed to predict the thermal and mechanical behaviour of the weldment and HAZ. The solution of non-linear transient problem is divided into two parts. Firstly, a thermal analysis [incorporating phase transformation effects] is performed to predict the temperature history of the model. Secondly, the predicted temperature field is applied as input for the subsequent mechanical analysis.

3.3.1 Coupling of Thermal and Mechanical Analyses

In a coupled analysis, thermal and mechanical behaviours are analysed sequentially in the time increments incorporating the effect of the mechanical work in the thermal evolution process. In the uncoupled thermo-mechanical problem, the thermal evolution results predicted by the

welding analysis can be independently verified prior to the mechanical analysis [Feng, 2005]. The degree of the finite element shape functions for the displacement is usually one order higher than that for the temperatures in order to have consistency between the two coupled modelling procedures. This is because temperature fields directly become thermal strain in the mechanical analysis [Lindgren, 2006]. The average temperature is used to compute a constant thermal strain to be applied as a thermal load in the mechanical analysis.

In this study, given the insignificance of mechanical work done compared to the thermal energy generated by the welding arc, the thermo-mechanical behaviour of the material during welding is simulated using the sequentially coupled formulation [Deng, 2009].

3.3.2 Thermal Analysis

Appreciating that temperature has a significant driving influence on the resultant microstructure, stress, strain and ultimately formation of distortions and other weld defects during the arc welding process; it becomes critically important therefore to accurately compute the transient temperature fields. During thermal analysis, it is assumed that the latent heat is evenly distributed during solidification or melting.

Heat Source Modelling

Consider a fixed Cartesian plane of (x, y, z) coordinates. A heat source located at $z = 0$ and at time $t = 0$ moves with constant velocity v along the z-axis. Figure 3.2 below gives a graphical illustration of the moving heat source model as suggested by Goldak *et al* (1984). The model follows a Gaussian distribution and has good features of density and power distribution control in the FZ and HAZ. Goldak's moving heat source model revealed that the temperature gradient in front of the heat source was lower than expected, while the trailing edge's gradient was steeper than revealed by experiments [Karunakaran and Subramanian, 2001]. Hence two ellipsoidal sources were combined to give the total heat flux as shown in figure 3.2 below.

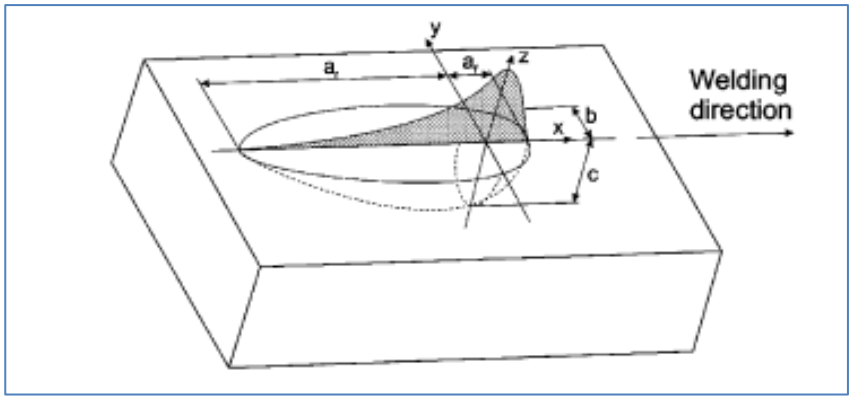

Figure 3.2: Goldak's Moving Heat Source Model

Source: Sattari-Far and Javadi (2008)

The corresponding heat input is estimated through the following equations:

$$q_r = \frac{6\sqrt{3Qf_r}}{\pi\sqrt{a_r bc}} \exp\left[-3\left(\frac{x^2}{a_r^2} + \frac{y^2}{b^2} + \frac{z^2}{c^2}\right)\right] \quad (3.1)$$

$$q_f = \frac{6\sqrt{3Qf_f}}{\pi\sqrt{a_f bc}} \exp\left[-3\left(\frac{x^2}{a_f^2} + \frac{y^2}{b^2} + \frac{z^2}{c^2}\right)\right] \quad (3.2)$$

where:

f_f and f_r are the front and rear fractions of the heat flux

a_f , a_r , b and c are semi-characteristic arc dimensions in the x, z and y directions respectively as depicted in figure 3.2

Values of b and c can be chosen as half-width of the fusion zone [Bang *et al*, 2002]. The z-coordinate is related to the moving coordinate as follows:

$$z = v(\tau - t) \quad (3.3)$$

where v is the welding speed, and τ is the lag factor that defines the position of the heat source at time $t = 0$

$$f_r = \frac{2a_r}{a_r + a_f} \; ; \; f_f = \frac{2a_f}{a_r + a_f} \; ; \; f_r + f_f = 2$$

$$Q = \eta EI \quad (3.4)$$

Where η = arc efficiency, E = welding voltage, and I = Welding current

Boundary Conditions

The heat transfer coefficients for convection and radiation are used to calculate the heat flux losses on the surfaces of the weld-piece using the following equations;

$$q_c = h(T - T_0) \quad (3.5)$$

$$q_r = \epsilon\sigma(T^4 - T_0^4) \quad (3.6)$$

where;

T_0 is the ambient temperature

T is the surface temperature of the weld pool

ϵ is the emissivity

σ is the Stefan-Boltzmann constant

h is the convection coefficient

Losses are not applied to the weld metal surface just under the arc while welding heat source is applied. Complete insulation is assumed in this case.

Modelling the Multi-pass Effect

The multi-pass effect in welding is modelled using the 'element birth and death technique'. The elements of each weld bead are meshed distinctly, and then linked to adjacent passes and the base metal mesh with contact surfaces. The weld metal elements and contact surfaces are de-activated at the commencement of the analysis, and reactivated at a specific time to simulate the bead addition sequence. [Bang *et al*, 2002].

Material Specification

The materials used in this study include ASTM A106 Grade B seamless high strength carbon steel pipe, ASTM A516 Grade 70 high strength low alloy pressure vessel plate, and the Afrox 7018-1 low hydrogen high strength filler metal. Table 3.1 below presents the mechanical properties for these materials.

Table 3.1: Mechanical Properties for the Materials

	UTS (MPa)	YS (MPa)	%EL	Poisson's ratio	Young's Modulus (GPa)
Plate	535	344	19	0.3	210
Pipe	510	260	31	0.3	210
Filler Metal	510	350	26	0.3	210

The chemical composition of base metals and the filler metal are tabulated in table 3.2 below. It can be observed from the said table that the chemical composition of all three materials is similar, and hence the equally similar material properties in table 3.1 above.

Table 3.2: Material Chemical Composition

	C	Si	Mn	P	S	Ni	Cr	Mo	Cu	V	Nb	Ti	Al
Plate Min/Max	0.197	0.307	1.03	0.011	0.0001	0.017	0.137	-	0.151	0.0012	-		0.027
	0.201	0.327	1.04	0.013	0.002	0.021	0.15	0.001	0.184	0.0014	0.001		0.037
Pipe Min/Max	0.198	0.24	0.79	0.009	0.004	0.05	0.09	0.011	0.08	0.001			
	0.30	0.26	1.06	0.035	0.035	0.40	0.40	0.15	0.40	0.08	0.01	-	0.041
Filler Metal	0.05	0.25	1.3	-	-	-	-	-	-	-	-	-	-
	0.09	0.45	1.5	0.025	0.025	0.01	0.06	0.03	-	0.02	-	-	-

Meshing

Fine mesh is used in the FZ and HAZ since high temperature gradients are expected in these regions. Element size is then increased as distance away from weld centreline increases. The 4-noded isoparametric quadrilateral elements are used.

3.3.3 Metallurgical Effects

During welding, the filler metal and base metal are melted at high temperature within the weld pool, subjected to solidification as they cool down, and then recrystallized – all within a thermal cycle. Meanwhile, the HAZ is also subjected to microstructural transformations due to high temperature gradients [Wang *et al*, 2009]. The temperature fields therefore determine the distribution and magnitude of welding-induced stresses and distortions through both thermal strains and phase transformation strains. Solid state transformation occurs during welding of steel.

It is well understood that transformation between body-centred cubic [bcc] form of iron [α – ferrite] and the face-centred cubic [fcc] form of iron [ϒ – austenite] is the main determinant of the microstructure and properties of steel. Phase transformation occurs when nuclei start forming randomly within the parent phase, i.e. nucleation. Such nuclei grow into particles and start consuming the parent phase and thereby developing a new phase. Thermo-mechanical processing methods of steel have been optimised over the years, in terms of parent metal properties. However, during welding the optimal base metal properties are altered due to localised thermal cycles [Elmer et al, 2003]. The inevitable result is the FZ and the HAZ whose microstructures differ from that of parent metal, thereby creating non-optimal properties in welded joints.

Lindgren (2006) observes that there are three generic options of dealing with the microstructural changes in numerical analysis, namely;

a. Ignoring microstructure changes completely. This is normally relevant if phase transformation takes place at high temperatures, and hence impact thereof on resultant residual stresses is considered negligible.
b. Accounting for microstructural changes in a simplified manner. Some authors, for example, use peak temperature and cooling rate $\Delta t_{8\text{-}5}$ as the only variables for determining microstructural changes.
c. Performing a full thermo-metallo-mechanical analysis, incorporating volumetric changes as result of phase transformation

In as far as the third option is concerned; a method that is widely used in accounting for solid state transformation during welding is that of using isothermal temperature-time-transformation [TTT] or continuous-cooling-transformation [CCT] curves to determine the evolution of transformation during the thermal cycle. CCT diagrams are used to predict the transformation that occurs during cooling in a thermal cycle; whereas TTT curves help determine the rate of transformation at a constant temperature. A typical CCT diagram for low alloy steel is given in figure 3.3 below. It should be observed that austenite forms once, during heating, the temperature increases above A_1; and it decomposes during cooling when the temperature falls below A_3. Similarly, depending on the cooling rate [i.e. $\Delta t_{8\text{-}5}$], ferrite, pearlite, bainite and/or martensite will form. Martensite forms at very rapid cooling rates.

Austenite – Ferrite Transformation

The decomposition of austenite into ferrite, pearlite or bainite is accomplished through a diffusive transformation process, i.e. the diffusion of carbon atoms. The reaction rate is controlled by diffusion of carbon atoms in the austenite phase under most conditions. [Elmer *et*

al, 2003]. This diffusion is described by the John-Mehl-Avrami-Kolmogorov [JMAK] law, which is given by equation 3.7 below. The utilisation of JMAK or Avrami equation to calculate the fraction transformed during cooling is in line with Scheil's additivity rule, which states that "*the fraction which transforms at any given temperature is a function of only the proportion of the metal already transformed and the temperature T*" [Anca et al, 2005]. The fractional volume of transformed material after a hold time at a given constant temperature is given by the following Avrami equation:

$$Y = 1 - \exp(-kt^n) \tag{3.7}$$

where;

n is the time exponent with a value between 1 and 4

$$k = \frac{\pi N G^3}{3} \tag{3.8}$$

k is a temperature-dependent time coefficient

N is the rate of nucleation per unit volume

G is the rate of nuclei growth into particles

The temperatures at which austenitic transformation begins during heating [A_1] and the one at which austenitic transformation is completed [A_2] can be worked out using the following equations [Deng,2009]:

$$A_1 = 723 - 10.7Mn - 16.9Ni + 29Si + 16.9Cr + 290As + 6.4W \tag{3.9}$$

$$A_3 = 912 - 203\sqrt{C} - 30Mn - 15.2Ni + 44.7Si - 11Cr + 104V + 31.5Mo - 20Cu + 700P + 400Al + 120As + 13.1W + 400Ti \tag{3.10}$$

Figure 3.3 shows the transformation of austenite into various phases [i.e. ferrite, pearlite, bainite and martensite] at corresponding cooling rates. It can be seen from the illustration that cooling the material at 0.33°C/sec will result to the formation of bainite over a wide range of cooling rate, and hence material thickness. Bainite formation will impede the formation of ferrite and pearlite, whose mechanical properties are less favourable [Ford and Scott, 2008]. The kinetics of the formation of ferrite, pearlite and bainite is the function of cooling rates during welding. However, the rapid cooling can suppress the formation of these phases and result in the development of a distorted lattice structure and the formation of martensite.

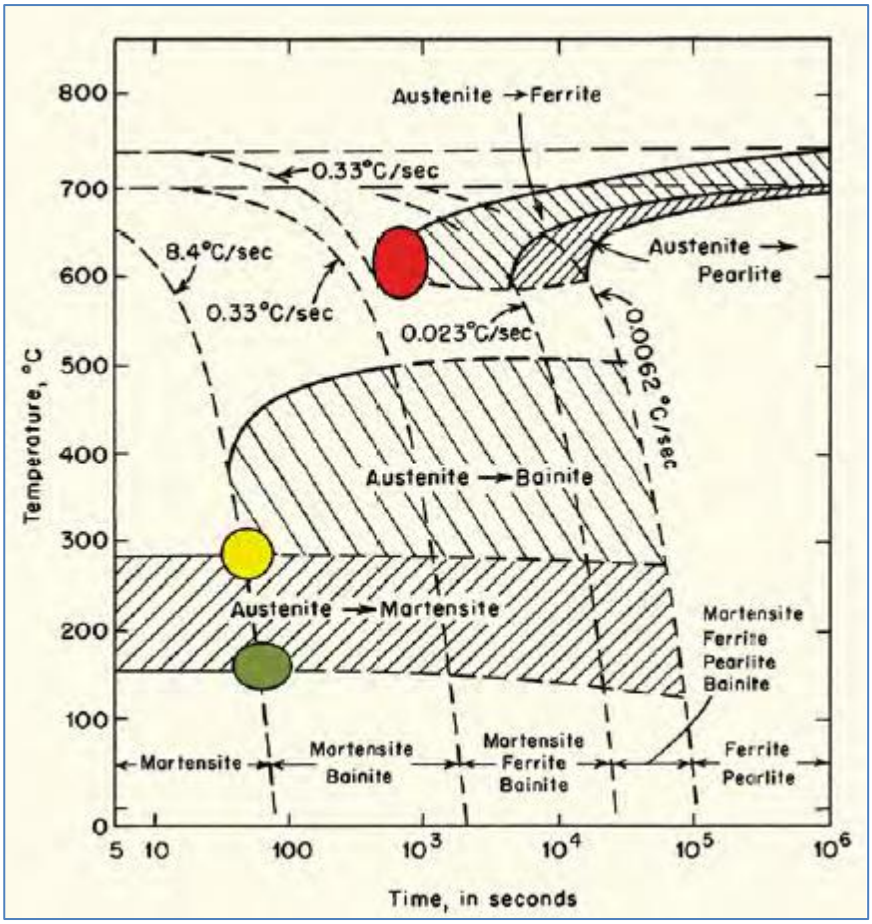

Figure 3.3. CCT Diagram for Low Carbon Low Alloy Steel

Source: Ford and Scott (2008)

NB: coloured circles represent sections discussed in the text

Martensitic Transformation

During cooling, when the temperature reaches M_s, austenite begins to transform into martensite. Figure 3.3 shows that martensitic transformation takes place at cooling rates higher than 8.4^0C/sec. This transformation is said to be diffusionless in that it occurs without the diffusion of carbon atoms, but instead it comes to pass through some form of cooperative, homogeneous movement of many atoms that results in crystal structure change. Given the diffusionless nature of the transformation, martensite inherits the chemical composition of the parent austenite. The formation of the body-centred tetragonal [bct], in a super-saturation form, results in the increased volume of the metal. The magnitude of the volumetric expansion in the FZ and the HAZ is dependent on the fractional volume of martensite transformed [Deng, 2009]. Martensitic transformation occurs through a time-independent process, and is not influenced by the cooling rate. Martensitic transformation cannot therefore be described by the Avrami

equation; instead the fractional volume can be calculated using Koistinen-Marburger law as follows;

$$y_m = Y_m\left[1 - \exp\left(-k(M_s - T)\right)\right]; T < M_s \quad (3.11)$$

Where;

Y_m is the residual volume fraction of austenite at Ms

k is the coefficient describing martensitic development as function of temperature [k = 0.011 for steels].

The data generated through the utilisation of both the Avrami law and the Koistinen-Marburger law is used to plot the CCT/TTT curves accordingly.

Figure 3.4 below illustrates the volumetric changes that occur during austenitic transformation [which takes place during heating], and the martensitic transformation [which occurs during rapid cooling]. The volumetric change as a result of rapid cooling-induced martensitic transformation, is evident through the rise in volume between temperatures M_s and M_f

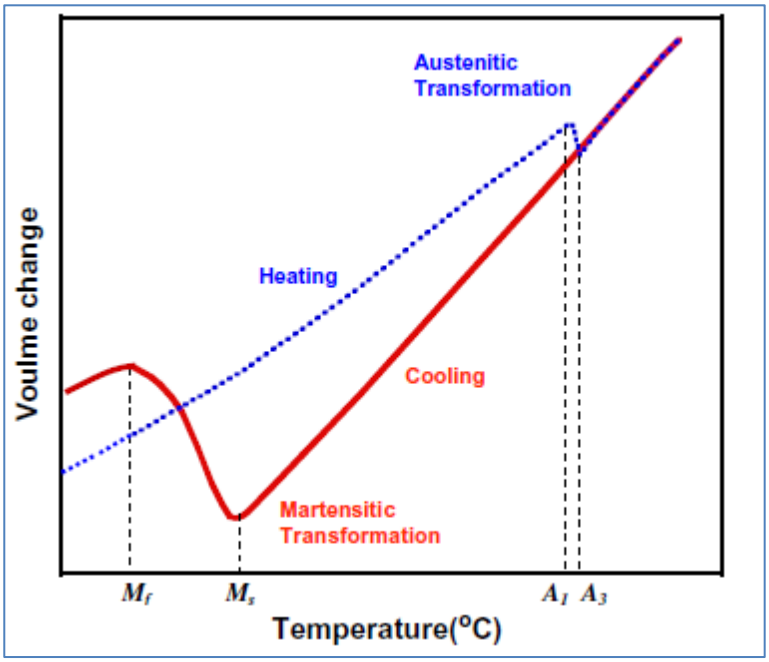

Figure 3.4. Schematic Illustration of Volumetric Change due to Phase Transformation

Source: Deng (2009)

The initial temperature M_s for carbon steel can be calculated using equation (3.12) below

$$M_s = 561 - 474C - 33Mn - 17Ni - 17Cr - 21Mo \quad (3.12)$$

3.3.4 Mechanical Model

Temperature histories from thermal analysis are given as inputs for the mechanical problem. The filler metal passes are tied to adjacent passes and the base metal with contact surfaces. Element birth technique can be skipped in this phase, due to significant numerical problems arising from the distortion of weld-pass elements during sequential activation [Bang et al, 2002]. Feng (2005) also observes that in a multi-pass weld joint, the root and cap weld passes usually dominate the formation of weld residual stresses and distortion. The fill passes have less influence on the final state of welding stresses and distortion, and therefore may be lumped together as one weld pass for purposes of FEA modelling [mechanical analysis], without compromising the accuracy of the results.

Thermo-mechanical analysis can be performed through one of the three constitutive models, namely elasto-plastic, elasto-viscoplastic and unified plasticity. Rate independent elasto-plastic models are the most frequently used in the simulation of thermal processes involving high heating/cooling rates [Simsir and Gur, 2008]. Therefore, during mechanical analysis, either the common rate-independent plasticity model – based on von Mises yield criterion – could be used, or the rate-dependant plasticity model. In this study the accumulated rate-dependent plasticity is neglected given the high temperature gradients experienced by the material during a relatively short thermal cycle. The pressure loading is left out in this study; only the thermal loading from the temperature histories is used. The thermal expansion coefficient is set to zero above melting temperature in order to prevent stress being applied to the liquid. The thermo-elastic-plastic constitutive model is developed to describe the deformation behaviour.

It is shown in Feng (2005) that the stress-strain constitutive equation is as follows:

$$\varepsilon_{ij}^{e} = \left[\sum_{I=1}^{N} \frac{1+\mathcal{V}_I}{E_I}\xi_I\right]\sigma_{ij} - \left[\sum_{I=1}^{N} \frac{\mathcal{V}_I}{E_I}\xi_I\right]\delta_{ij}\sigma_{kk} + \delta_{ij}\int_{T_0}^{T}\sum_{I=1}^{N}\alpha_I\xi_I dT + \delta_{ij}\sum_{I=1}^{N}\beta_I\left(\xi_I - \xi_{I_0}\right) \quad (3.13)$$

$$\varepsilon_{ij}^{i} = G\left[\frac{\partial F}{\partial \sigma_{ij}}\sigma_{kl} + \frac{\partial F}{\partial T}T + \sum_{I=1}^{N}\frac{\partial F}{\partial \xi_1}\xi_1\right]\frac{\partial F}{\partial \sigma_{ij}} \quad (3.14)$$

where, $E_I, \mathcal{V}_I, \alpha_I, and\ \beta_I$ represent Young's Modulus, Poisson's ratio, coefficient of thermal expansion and dilatation of the *i*-th constituent respectively. And *G*, *F*, $\sigma\ and\ \xi$ correspond to Gibbs free energy, yield function, stress and structural fraction respectively.

3.4. Finite Element Modelling

A sequentially-coupled thermo-mechanical problem, with metallurgical effects, is considered in this study. The problem is simplified as an axisymmetric 2D analysis, which is performed using the ABAQUS® code, version 6.11. Figure 3.5 shows the steps taken in the modelling process. First, the thermal analysis is performed, incorporating metallurgical effects; and then the subsequent mechanical analysis takes place.

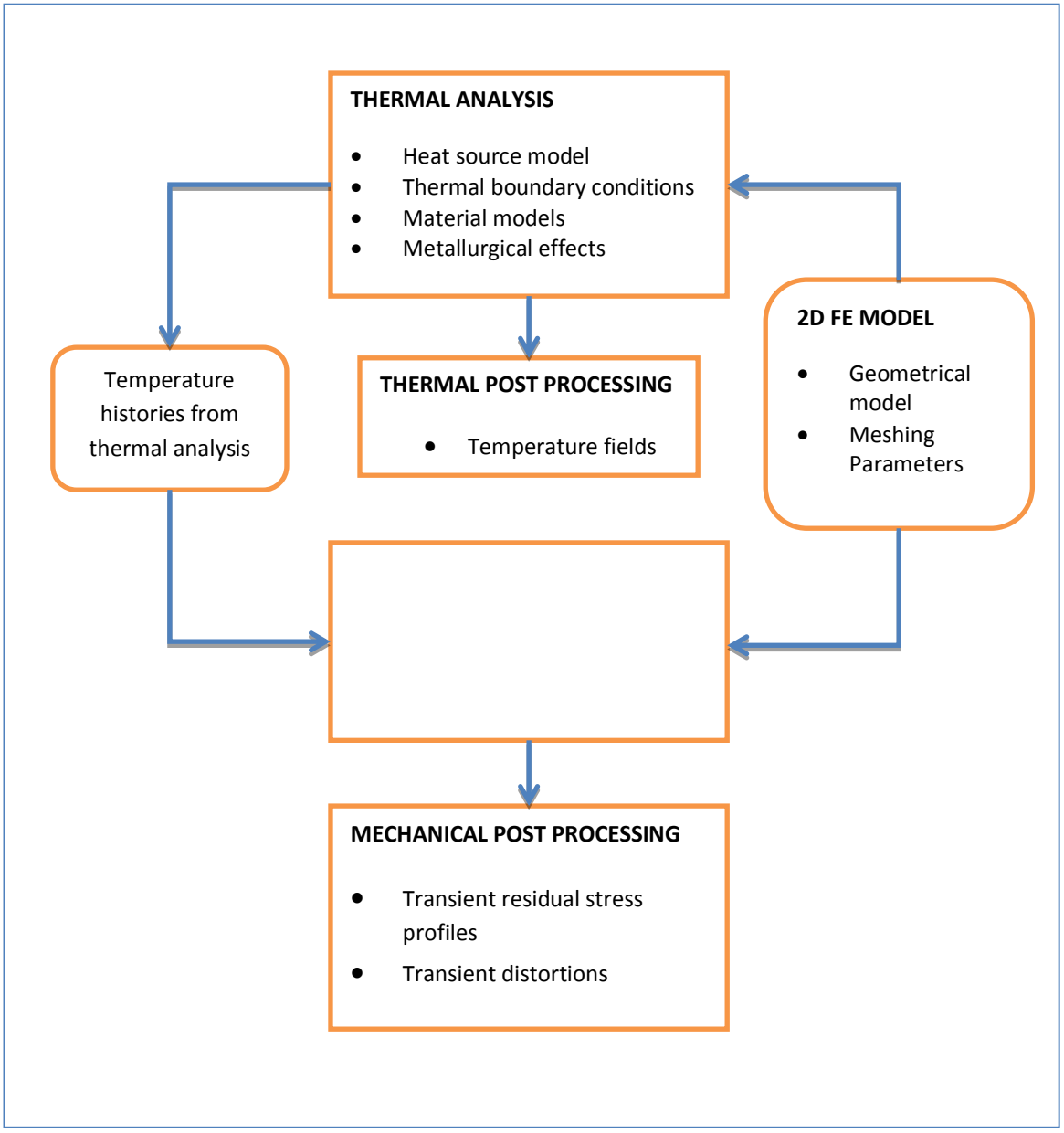

Figure 3.5. Overview of the Thermo-Mechanical Analytical Procedure

Source: Qureshi (2004)

Figure 3.6 below shows the axisymmetric model developed to solve the thermo-mechanical problem. There are four weld passes as indicated in the schematic, and the dimensions of each weld pass is known so that proper calculations of the volumetric body heat flux per weld pass could be performed.

It can be seen in figure 3.6 that the pipe and plate are joined through a full-penetration four-pass butt-weld. The dimensions of each weld pass are known, and are used to calculate the volumetric heat flux transferred to the weld-piece during welding. The "element birth and death" technique is used to model the multi-pass weld.

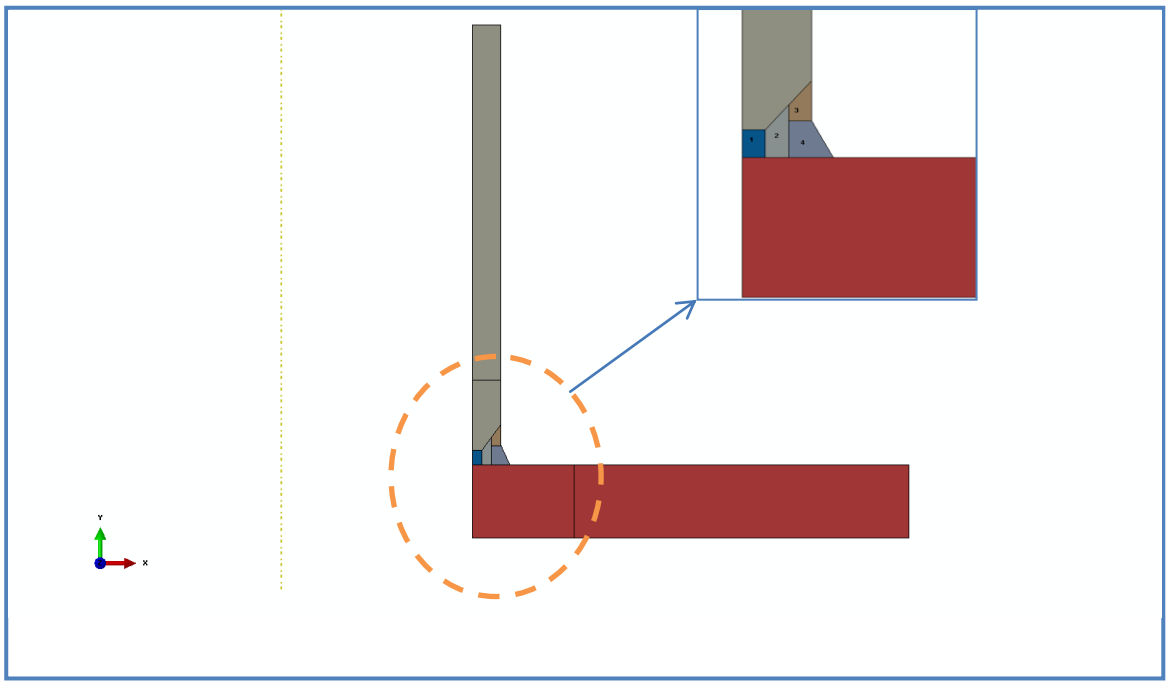

Figure 3.6. The Axisymmetric FE Model

3.4.1 Modelling Assumptions

Axisymmetry refers to a condition where welding heat is deposited at the same time around the circumference of the weld. This assumption is common amongst circumferential multi-pass welding applications as it reduces the size of the FE model and computational time significantly [Bang et al, 2002]. The ***latent heat*** of fusion is taken as 2.7×10^5 J/kg at solidus and liquidus temperatures of 1440^{o}C and 1550^{o}C respectively, and is used to model the solid-liquid transformation. Heat losses are not applied to the weld metal surface just under the arc while welding heat source is applied. Complete insulation is assumed in this case.

3.4.2 Thermal Analysis

The body heat flux is calculated for the axisymmetric model using equations 3.1, 3.2, 3.3 and 3.4 for each weld bead. The dimensions of the weld beads are used to calculate the exact volume of the melted pool so that it can be used for heat input calculations. The ambient temperature of 21^{o}C is applied throughout the calculations, as was recorded in the experiments. The heat rate required to raise the temperature of weld-piece from 21^{o}C to 1500^{o}C was then calculated using the above information, and inputted into the axisymmetric model as heat input per weld pass. The emissivity of 0.625 and convection coefficient of 15 W/m^{2}.K were used for boundary conditions throughout the thermal analysis. The Stefan Boltzmann constant was taken as 5.67x10^{-8}. The axisymmetric model allows for the 'lumping' of the entire heat quantity during the heating cycle. The calculated volumetric flux shown in table 3.3 was therefore inputted into the model as a lumpsum for the duration of the weld-pass heating cycle.

Table 3.3: Heat Input Parameters of Each Weld Pass

Weld Pass	Volume m^{3} (x10^{-7})	Cycle Time (heat + cool) s	Volumetric Flux J/m^{3}.s (x10^{10})
1	4.39	80	5.53
2	6.45	94	4.42
3	4.70	77	4.98
4	8.91	75	2.56

The volumetric change due to phase transformation was considered through incorporating the temperature-dependant material properties that correspond to the actual phases of the material at corresponding temperatures. Lingamanaik and Chen (2011) established that the thermal conductivities of austenite and martensite can be determined using the equations below.

$$\lambda\,(austenite) = 0.016 + 1.3x10^{-5}\,x\,T \tag{3.15}$$

$$\lambda\,(martensite) = 0.025 + 3x10^{-6}\,x\,T \tag{3.16}$$

Similarly, the values of specific heat for austenite and martensite are given by the equations below

$$C\rho\,(austenite) = 370 + 0.298\,x\,T \tag{3.17}$$

$$C\rho\,(martensite) = 450 + 0.387\,x\,T \tag{3.18}$$

In order to match the appropriate material phases to the corresponding properties, the austenite properties are used between A_3 and A_1 temperatures, and martensite properties are used between M_s and M_f temperatures. Austenitising temperatures are determined using equations 3.9 and 3.10, whereas the martensitic transformation temperatures are worked out through equations 3.11 and 3.12. The resultant values are given in table 3.4 below

Table 3.4: Austenitising and Martensitic Transformation Temperatures

Temperature ^{0}C	Plate	Pipe	Filler Metal
A3	823	816	845
A1	723	719	721
Ms	429	367	467
Mf	232	170	270

The temperature-dependant material properties were calculated using the equations 3.15 to 3.18 above, as well as the values given in table 3.4. Figure 3.7 below illustrates the outcome of such calculations.

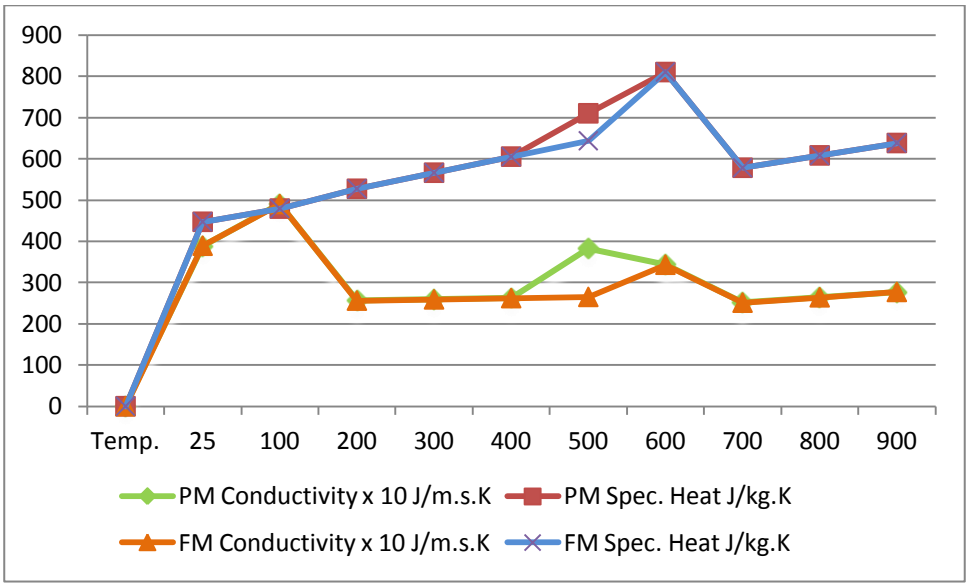

Figure 3.7. Temperature-dependant Material Properties

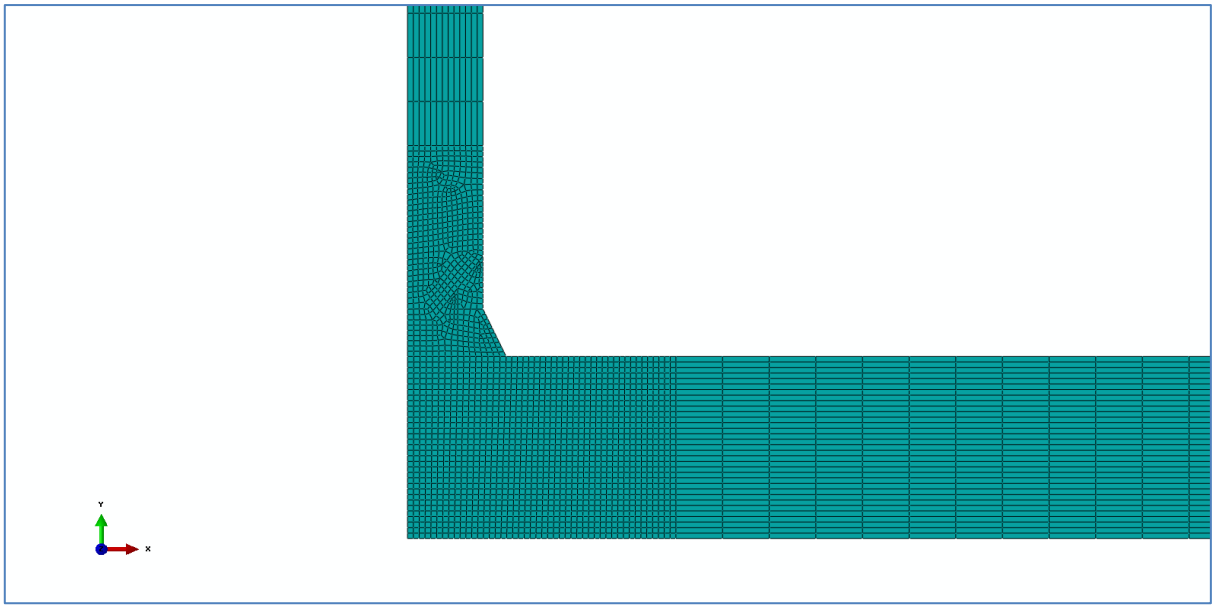

Figure 3.8. The Mesh of the Axisymmetric Model

The parent metal (PM) and filler metal (FM) material properties are plotted against temperature to shown the variation of the former as temperature increases. It can be seen that the properties of the two metals are fairly similar. The pipe and plate material was taken as similar for the purposes of the above analysis.

The DCAX4 element type was used to produce the mesh as shown in figure 3.8. The finer mesh was used for the FZ and HAZ regions given the high temperature gradients that exist there. The mesh size increases as the distance away from the weld centre-line increases.

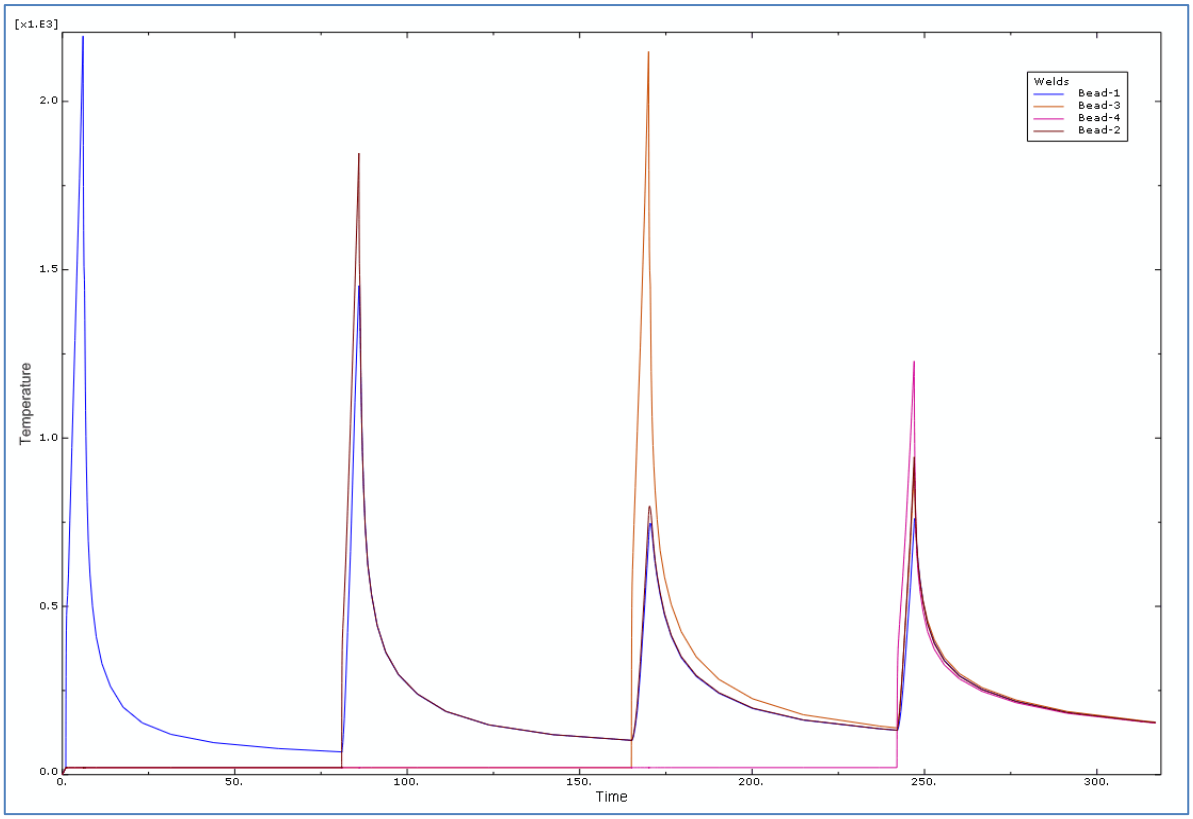

Figure 3.9. Temperature Distribution Across the Weld Metal

Temperature distribution schematic in figure 3.9 shows temperatures registered from the centre of each weld bead. The nodes were chosen from each weld bead and their temperatures plotted against time as shown. It can be seen that temperatures of up to 2300^{o}C are reached in the weld-pool as a result of the heat input. The inter-pass temperatures range between 100^{o}C and 200^{o}C. The relatively lower peak temperature reached during the fourth pass is due to the lower volumetric heat flux generated during this pass. The temperature histories are subsequently used as the only loading in the stress analysis problem.

3.4.3 Mechanical Analysis

The thermo-elastic-plastic model is developed based on von Mises yield criterion in order to describe the residual stress distribution and distortions. Thermal loading from the preceding thermal analysis is used as input into the mechanical model. The rest of the model is similar to the thermal model, except for the elements that were made one order higher in the stress analysis than the previous analysis.

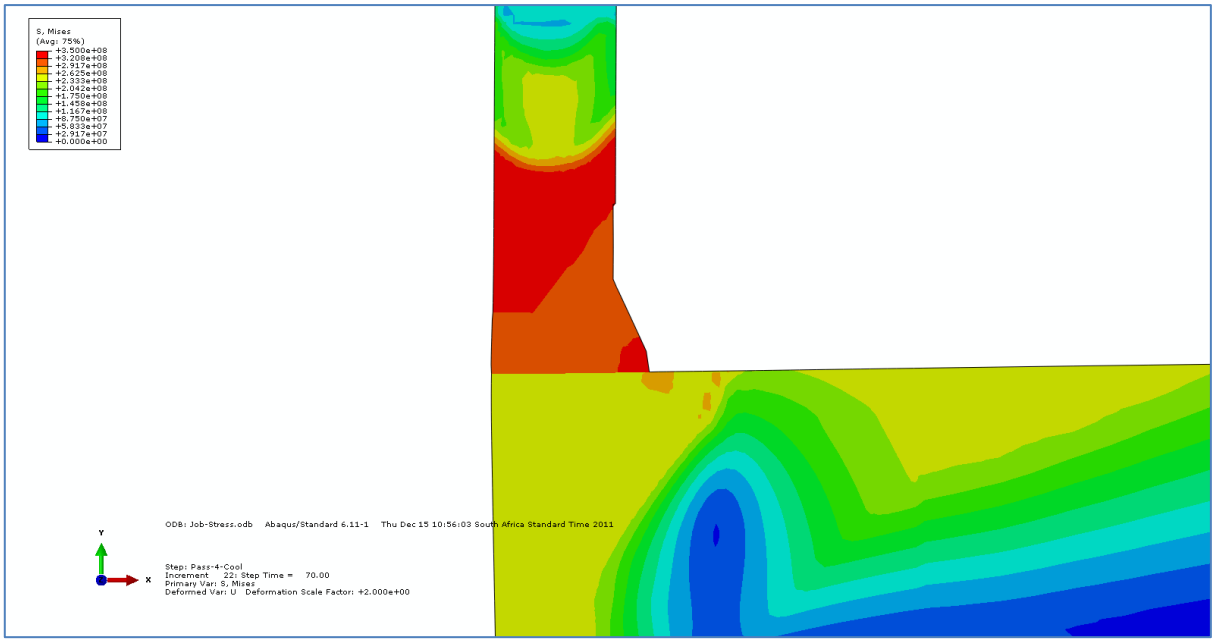

Figure 3.10. Von Mises Stress Distribution

The above von Mises mapping illustrates the stress distribution after the cooling stage of the final weld pass. It can be seen that tensile residual stresses as high as the material yield strength are experienced in the FZ and HAZ of the weld immediately after cooling. The stresses disappear as the distance away from the weld centre-line increases.

Radial residual stresses are quite high [in the region of 337 MPa] in the HAZ of the plate side of the weld-piece as shown in figure 3.11(a). This value is quite close to the yield stress value of 344 MPa for the plate material. Axial stress values are highly tensile on the inside of the pipe close to the HAZ, and in the CGHAZ region of the plate side, while the external surface is under compressive stress.

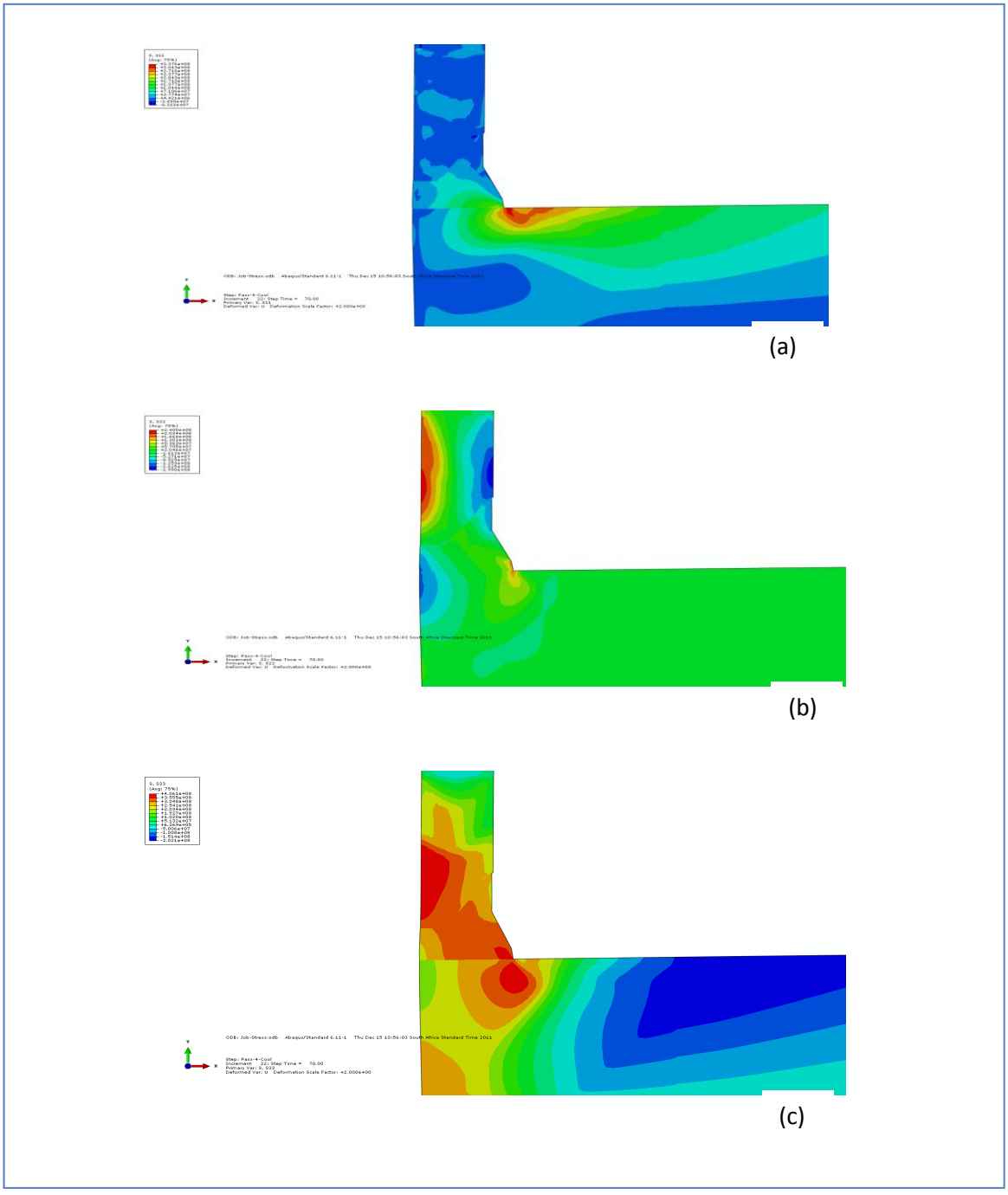

Figure 3.11. Residual Stress Distribution, (a) Radial, (b) Axial, (c) Hoop

Tensile hoop stresses exists in the FZ and HAZ of the weld-piece, whilst compressive stresses exist further away from the weld centre-line. It appears therefore that the internal surface is generally under tensile stress, while the external surface is under compressive stress.

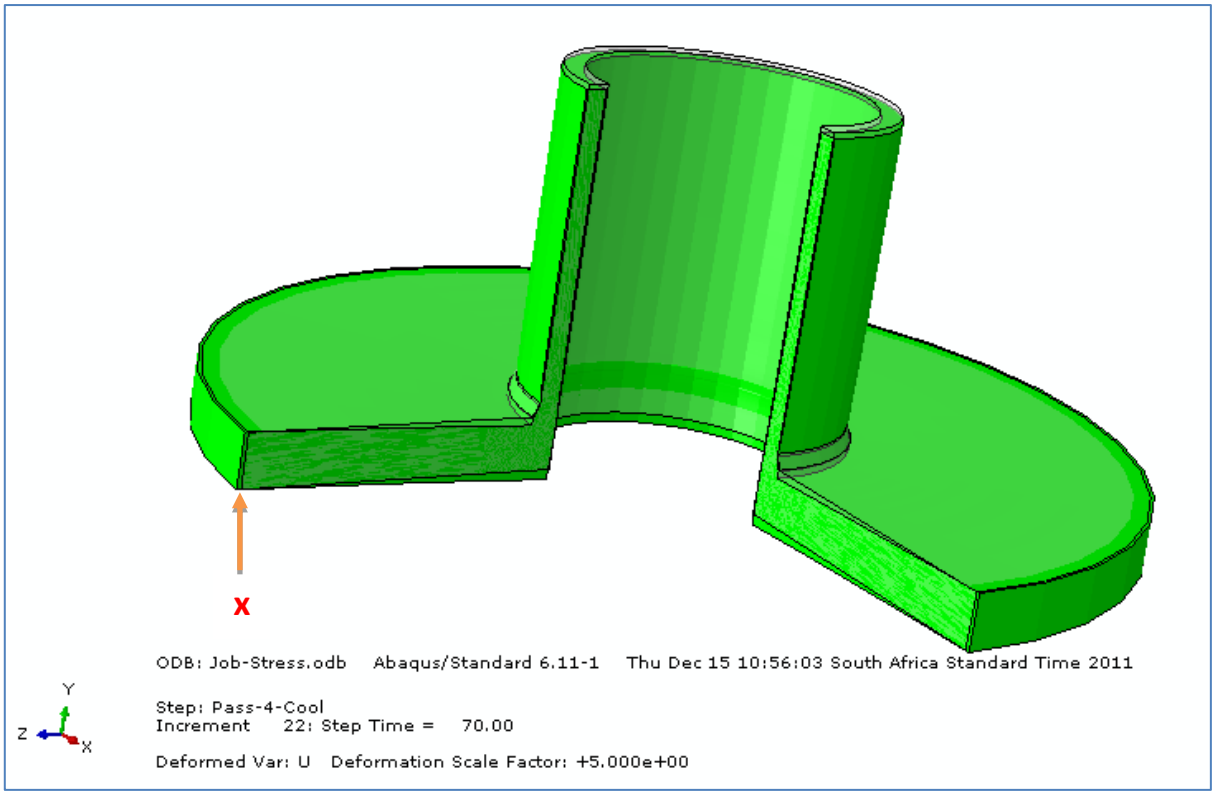

Figure 3.12. 3D Deformed Shape of the Weld-piece

The 3D illustration in figure 3.12 shows the extent of deformation from the original shape dimensions. It must be noted that the weld-piece was constrained at point ‘x’, and all the other points were free to move. Movement in the axial ‘y’ direction is conspicuous from the figure.

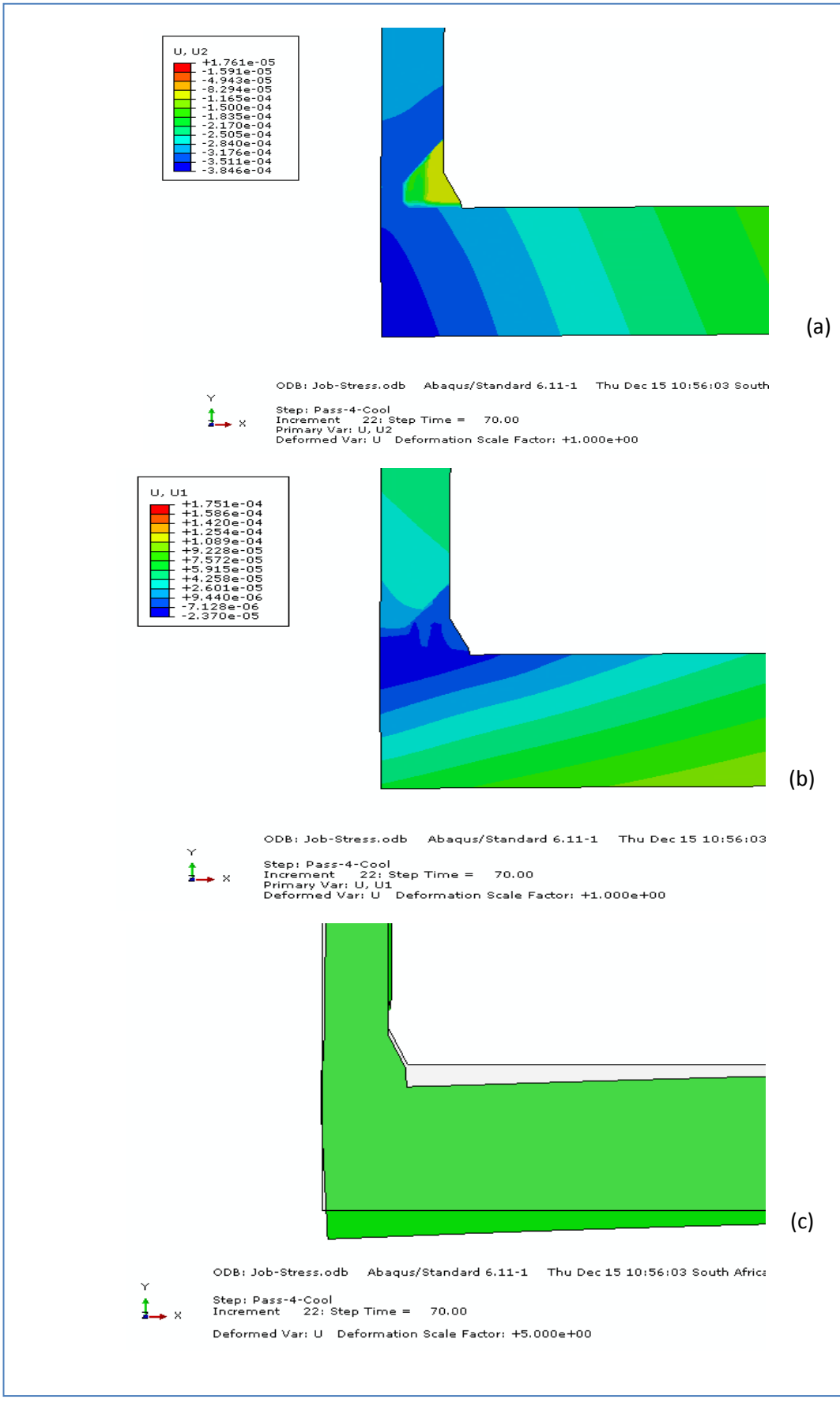

Figure 3.13. Contours for Axial and Radial Distortions

The deflection of the welded structure is clearly visible in the contours shown in figure 3.13. Deflections of up to 0.384mm in the axial direction, and 0.0237mm in the radial direction are observed. The weld-piece was 'pulled' down in the axial direction as cooling took place. This is visible in both sketches (a) and (c) in figure 3.13. Radial shrinkage around the FZ and HAZ is clearly visible in sketch (b). Although the magnitude of the deflection is significantly magnified, it is however still clear that welding induces distortions and changes in dimensions of the welded structure

Chapter 4

Experimental and Empirical Analysis

It was mentioned in chapter one above that the methodology adopted in this study involves a hybrid of numerical analysis, empirical calculations and validating experiments. This chapter discusses the experiments and empirical calculations performed in order to validate the numerical simulations discussed in the preceding chapter. The experimental work includes the work physically performed at the mechanical workshop and the testing laboratory, as well as extracts from previous similar studies where physical experiments could not be performed due to lack of facilities.

4.1 Weld-piece Preparation

Two weld-pieces were prepared according to the geometry given in figure 4.1 below. Table 4.1 gives the welding conditions that existed during the preparation of the weld-piece specimens.

Table 4.1: Welding Conditions

Welding Conditions
Room temperature: 21^{o}C
No preheat
Cooling at room temperature
Welding procedure: SMAW
High strength pressure vessel plate 252 x 252 x 10mm
2" seamless carbon steel pipe chamfered @ 45^{o}
Root gap of 2mm
AWS A5.1.91 E7018-1 H8 low hydrogen electrode – 3.15mm

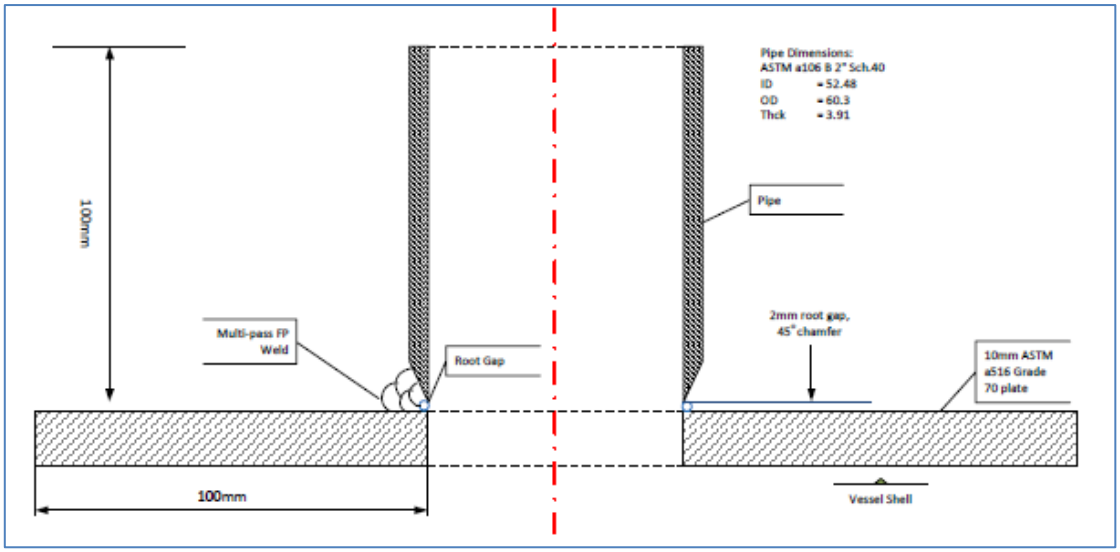

Figure 4.1: The Weld-piece Geometry

The high strength carbon steel pipe is welded onto the pressure vessel plate of similar strength using low hydrogen high strength E-1708 electrodes. Materials ASTM A106 and ASTM A516, for the pipe and plate respectively, were chosen for practical purposes since these materials are typically used for pressurised system application. A hole of the same size as the internal diameter of the pipe was drilled through the plate [figure 4.2 (a)] in order to position the pipe in the same way that the nozzle would be positioned on the pressure vessel. The root gap of 2mm was attained through mounting the pipe on the plate by inserting a 2mm steel rod in between the pipe and the plate [figure 4.2 (b)], and placing four equi-spaced tag welds around the weld groove. A four pass full penetration weld was then performed using the SMAW process [figure 4.2 (c) and (d)].

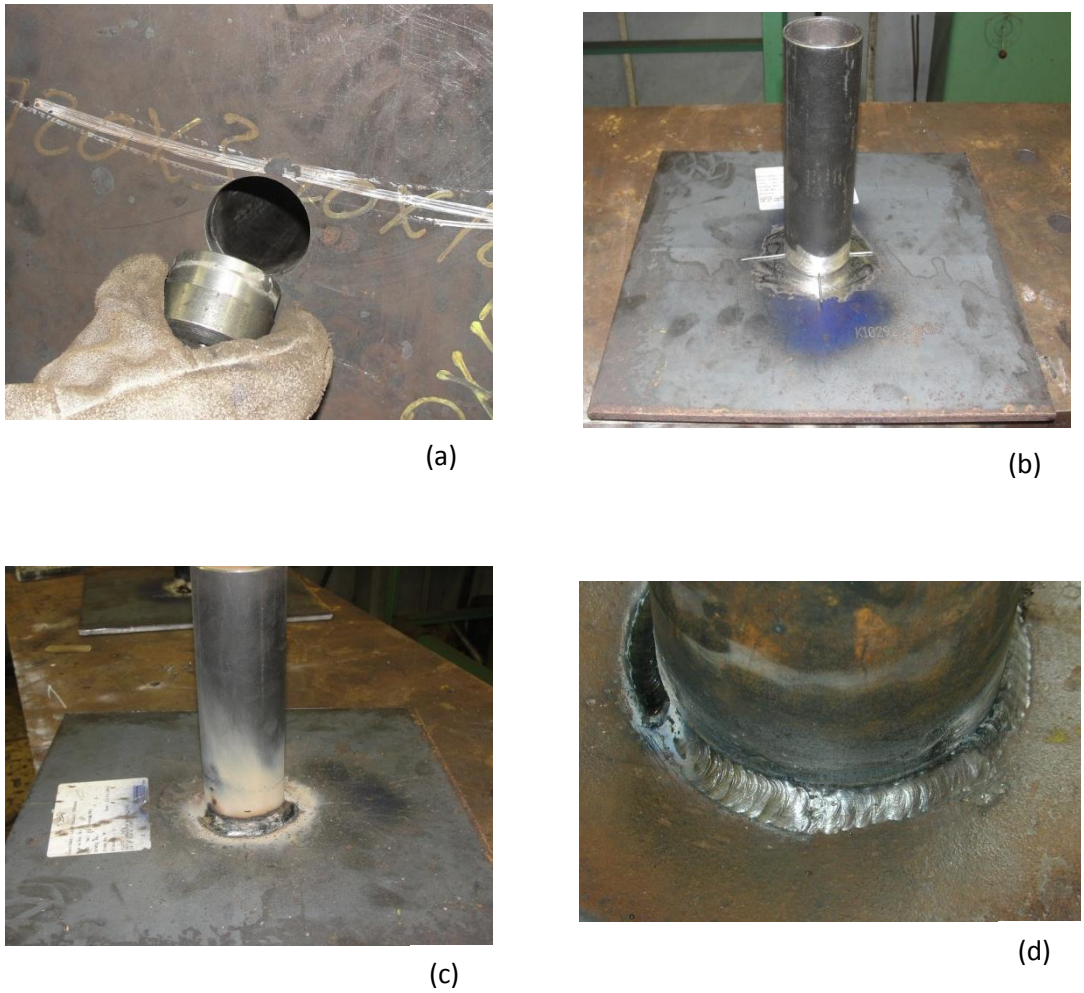

Figure 4.2: Preparation of the Weld-piece

4.1.1 Equipment Used

A Miller TIG Welder, model 330A/BP was used for welding the above material. The machine can be used on either the TIG mode or the SMAW mode; all that has to happen is to either place the selector on DC- [TIG] or DC+ [SMAW] positions. The current was set at 67.5A and the voltage of 30V was supplied through a three-phase source. Figure 4.3 shows the front of the welding machine.

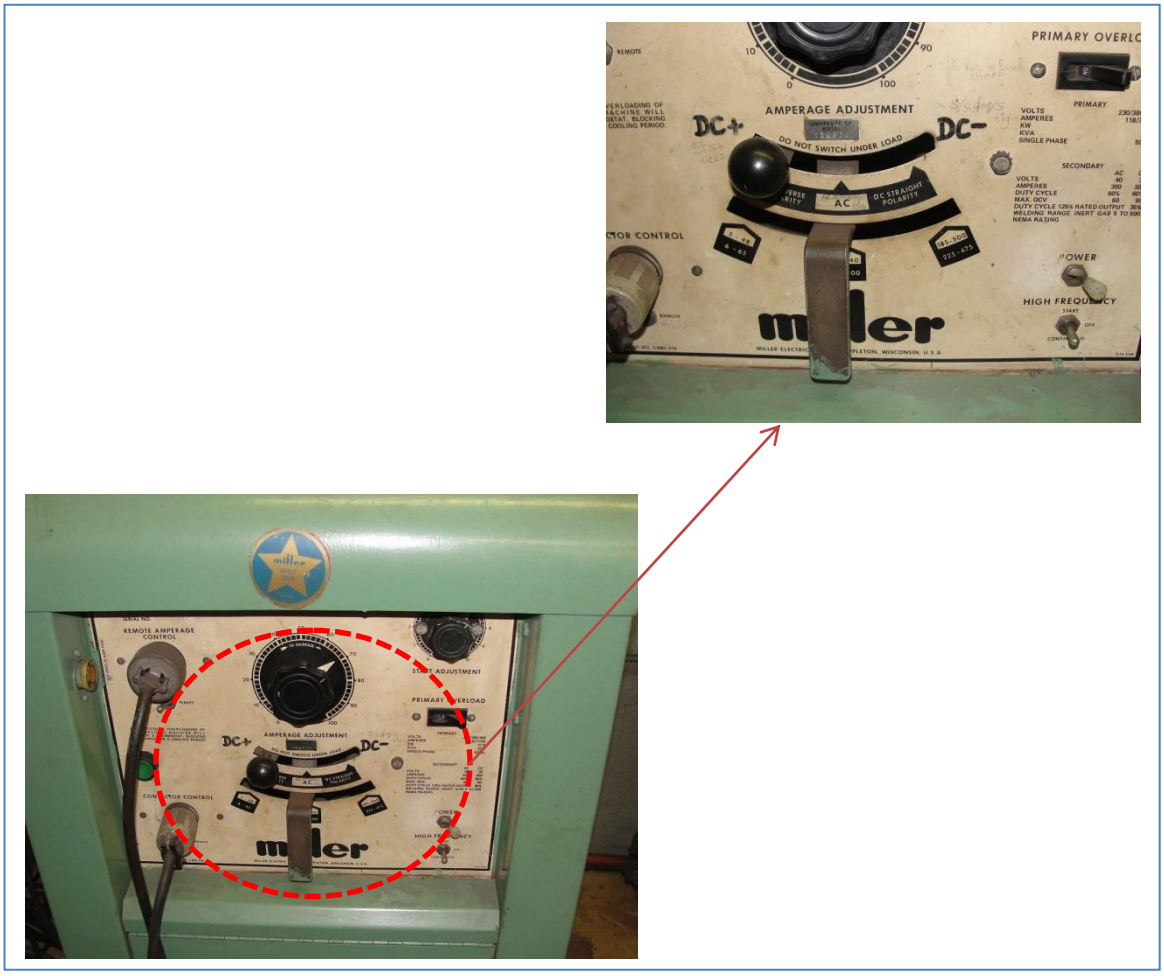

Figure 4.3: The Miller A330/BP TIG Welding Machine

Temperature was measured using the Sentry ST677 HDS infrared thermometer, with a temperature range of 32 to 1650^{o}C, an accuracy of 2%, a response time of 500 milliseconds, and a distance/spot ration of 50:1. This is shown in figure 4.4

Figure 4.4: The Sentry ST677 Thermometer

4.1.2 Welding Outputs

As mentioned above, four weld passes were performed. During each weld pass, temperature measurements were taken in the weld-pool; and just before commencement of the subsequent weld pass, inter-pass temperature measurements were recorded. Table 4.2 gives details of the welding outputs.

Table 4.2: Welding Outputs

Pass	Voltage V	Current A	Interp. Temp C	Weld Temp C	Speed mm/s	Filler Metal	Cycle Time s	Interp. time s
1	30	67.5	21	1571	2.37	3.15mm	80	90
2	30	67.5	118	1563	2.06	3.15mm	94	65
3	30	67.5	170	1592	2.46	3.15mm	77	52
4	30	67.5	189	1587	2.53	3.15mm	75	45

4.2 Structure of Experiments

Experiments are conducted in order to ensure reliability of numerical simulations [i.e. Finite Element Analysis] and to extend the utility of the research work to practical applications. Three main types of validation categories are performed as given in Figure 4.5.

4.2.1 Thermal Model Validation

For weld thermal model validation, two types of experimental approaches are employed. The first approach is based on temperature measurement through infrared thermometer as described in section 4.1 above. Temperature distributions of sections away from the Fusion Zone (FZ) and in the Heat Affected Zone (HAZ) are measured experimentally and compared with the Finite Element Analysis (FEA) data at the corresponding locations. In order to match the experimental data, Finite Element (FE) models can be calibrated by varying the welding process parameters accordingly.

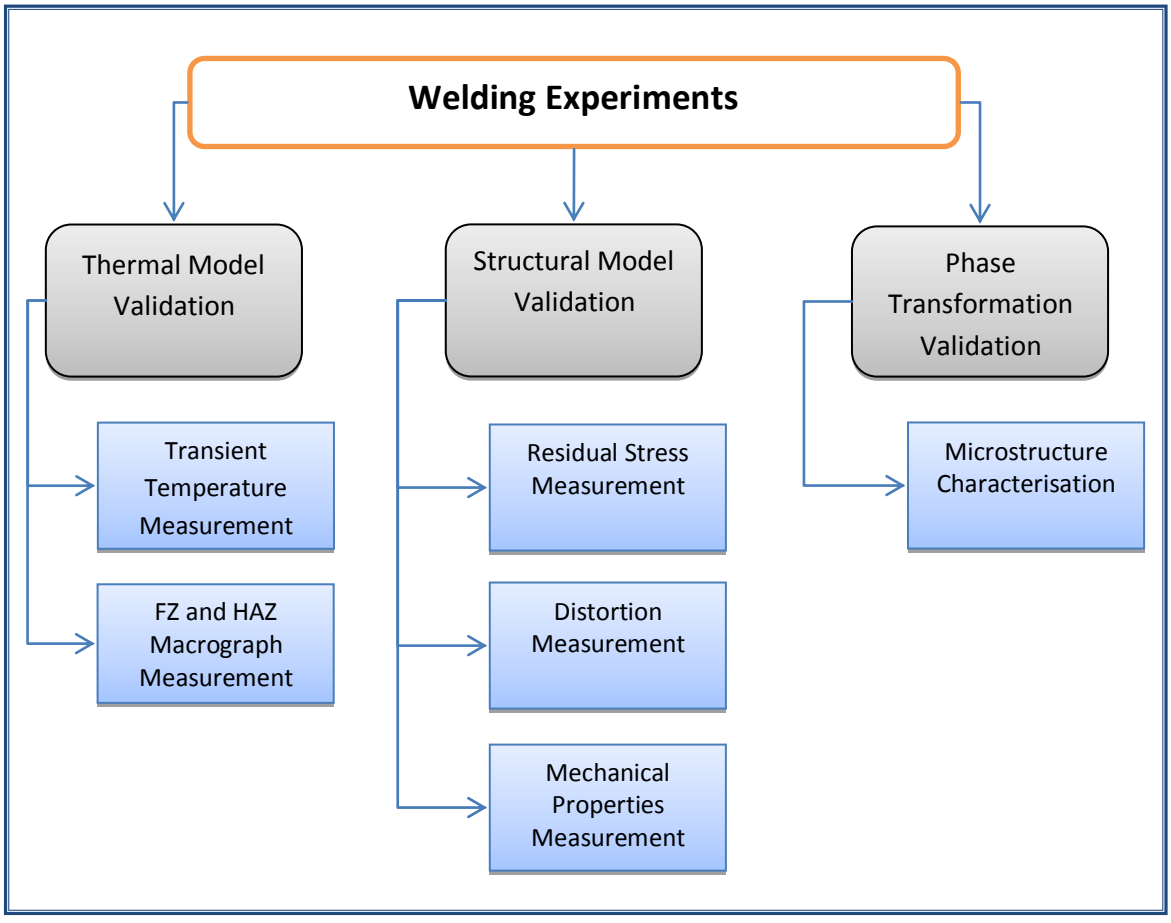

Figure 4.5: Schematic Illustration of Validation Experiments

The recorded temperatures in table 4.2 above are in agreement with the FE temperature fields shown in figure 3.9 above. Both peak and inter-pass temperatures are not too far from the measured values.

The second approach is the comparison of FZ and HAZ from experimental macrograph. In order to avoid undesired heat effects, samples were cut by using laser cutting. Samples were also cut well away from start/end and tack weld locations. For FZ and HAZ macrograph measurement, the following steps were taken:

a. Sample preparation by laser cutting

b. The sample was mounted on resin cast

c. Sequential grinding by using silicone carbine abrasive paper with varying grit sizes [300, 500, 800, 1000]

d. Diamond paste polishing with particle sizes of 9 µm, 6 µm, 3 µm, and 1 µm.

e. Etching the sample with 2% nital solution for 30 seconds and rinsing with alcohol

f. Study the sample to reveal HAZ and FZ dimensions

Figure 4.6 shows the macrographs observed from a few specimens that were prepared according to the procedure stipulated above. The transition zone is clearly visible in (a) and (b), such that one can see the change from weld metal to parent metal. The HAZ is shown at different directional planes in (c) and (b), and the effect of high temperature exposure is quite evident.

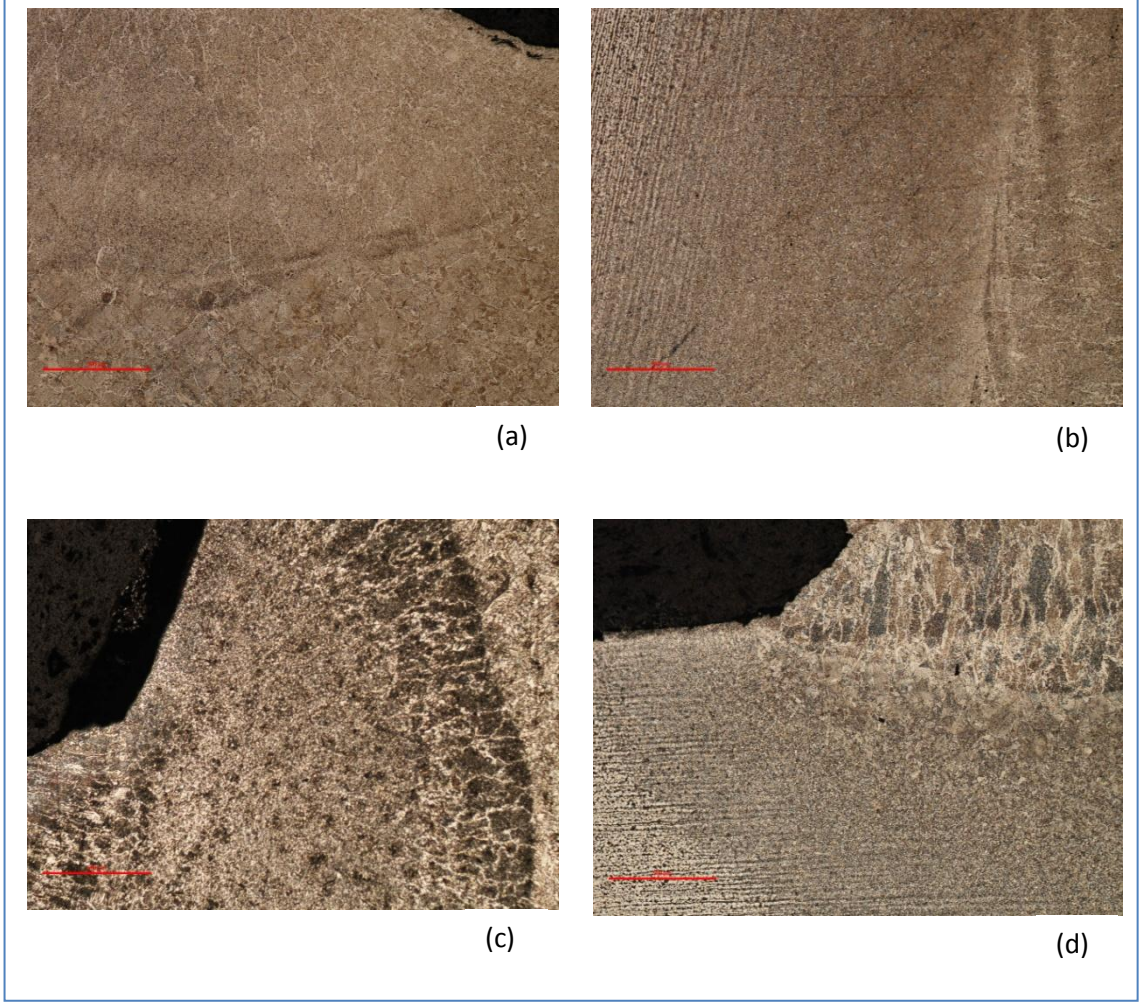

Figure 4.6: The FZ and HAZ Macrographs. (a) Transition Zone on Pipe Side; (b) Transition Zone on Plate Side; (c) HAZ on Pipe Side; (d) HAZ on Plate Side

4.2.2 Structural Model Validation

As illustrated in figure 4.5, both residual stress and distortion measurements must take place in order to adequately validate the weld structural model. For distortion, transient axial and residual radial distortions are measured on weld specimens. Furthermore, hoop and axial residual stresses are also measured on the same weld specimens in order to obtain comparable results.

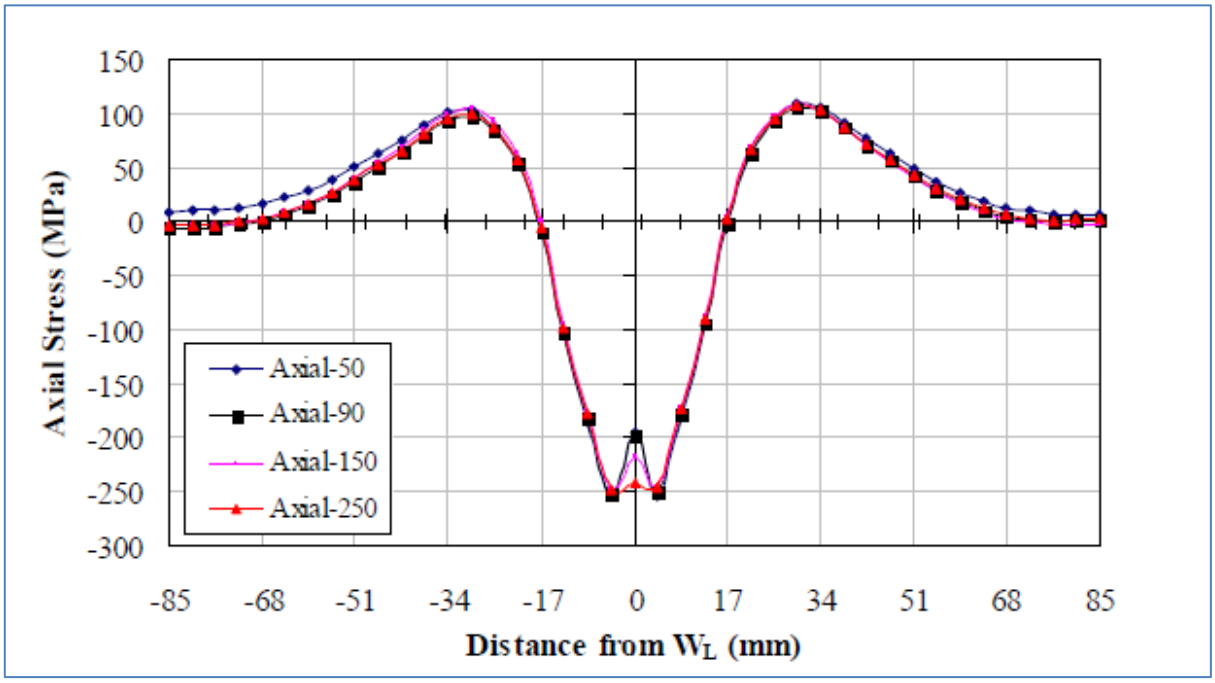

Figure 4.7: Residual Axial Stress Distribution on the Outer Surface

Source: Qureshi (2004)

Residual stress can be measured by hole-drilling method. The Mathar – Soete hole drilling strain measurement technique is widely used and has acceptable accuracy. As the hole is drilled on to the material, residual strain is released, and the change in strain is measured. ***Electrical strain gauges*** are used for measuring the changes in strain along the number of locations on the weld-piece. Three strain gauges are normally positioned 120-Degree from each other around the circumference of the measuring point on the weld-piece. Once the strain values are known, residual stress is calculated using the standard stress/strain formulae. Results are then displayed in the graphical format to show the changes in residual stress as the location drifts away from the weld fusion zone.

Due to lack of hole-drilling technique facilities, for the purposes of this study, data from previous similar experiments is used to validate the FE model. Qureshi (2004) performs a study to analyse residual stress and distortions in thin-walled cylinders using FE methods and experiments. The material used in the study is low carbon steel AH36, whose chemical composition is similar to the material used in the present study. The results of Qureshi's experiments are therefore used for the purposes of validating the structural model [residual stress and distortions] of the present study.

Qureshi used the hole-drilling method to measure the residual stress and a dial indicator to measure distortions. Figure 4.7 shows the distribution of the axial residual stress on the outer surface of the cylinder at different circumferential locations from the weld start position [i.e. at 50, 90, 150 and 250 degrees from weld start]. It is observed that at the weld centre-line, the compressive axial stresses are at their highest value [i.e. up to -250 MPa], which is close to the yield stress of the weld metal material. As the distance from the weld centre-line increases, the magnitude of the compressive axial stress decreases all the way to zero, and eventually changes direction to tensile as distance grows even further away from weld centre-line. The axial stress distribution on the inner surface of the cylinder is almost a mirror image of the outer surface stress profile.

The hoop residual stress distribution is shown in figure 4.8. It can be observed that the hoop stresses are virtually zero at the weld centre-line, increase to the maximum tensile value as distance away from the weld centre-line increases, then decreases back to zero before changing direction to compressive further away from the weld centre-line. The compressive stress peak values are higher than the tensile stress peak values. The hoop stress distribution profile of the inner surface is similar to that of the outer surface except that the tensile stress peak values are higher than compressive stresses. It therefore follows that the outer surface is under compressive residual stress, while the inner surface is under tensile stress.

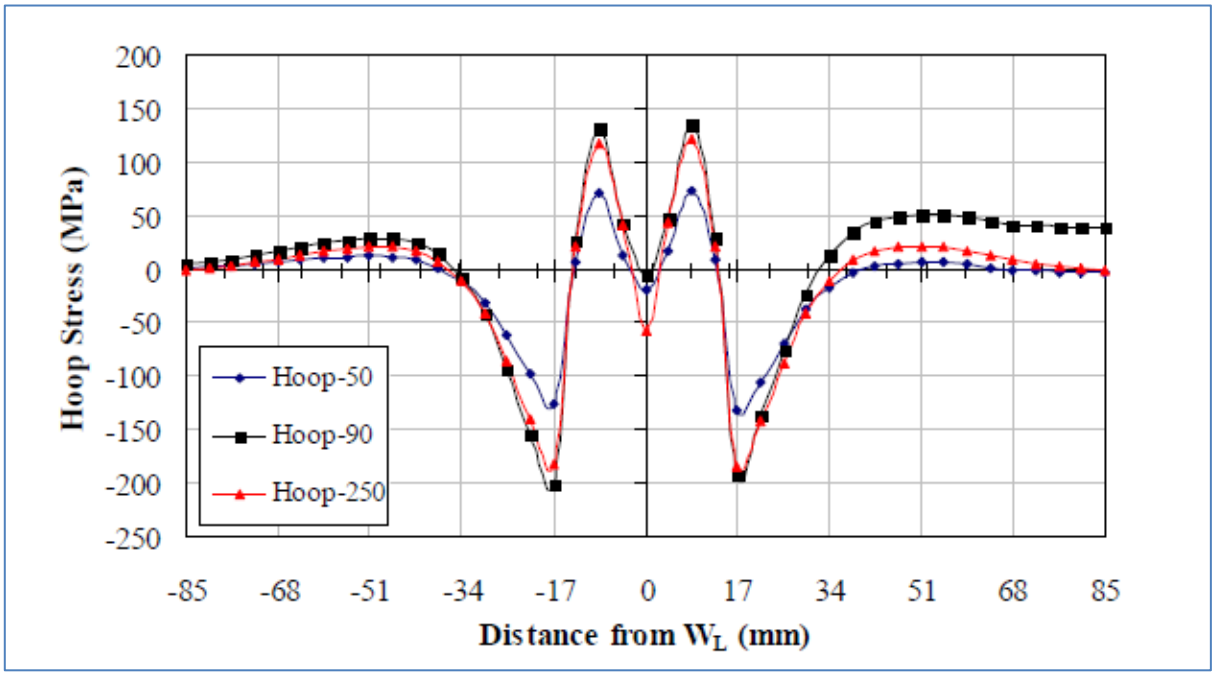

Figure 4.8: Residual Hoop Stress Distribution on the Outer Surface

Source: Qureshi (2004)

Qureshi's study reveals that maximum axial and radial deflection occur near the weld centre-line. Axial face tilt ranging from -0.34 to 0.23mm is observed on a 300mm diameter cylinder of 3mm thickness. The axial shrinkage decreases as distance away from weld centre-line increases. Minimum axial shrinkage, which is close to zero, is observed at the restrained end, whereas the restraint-free end experiences some deflection.

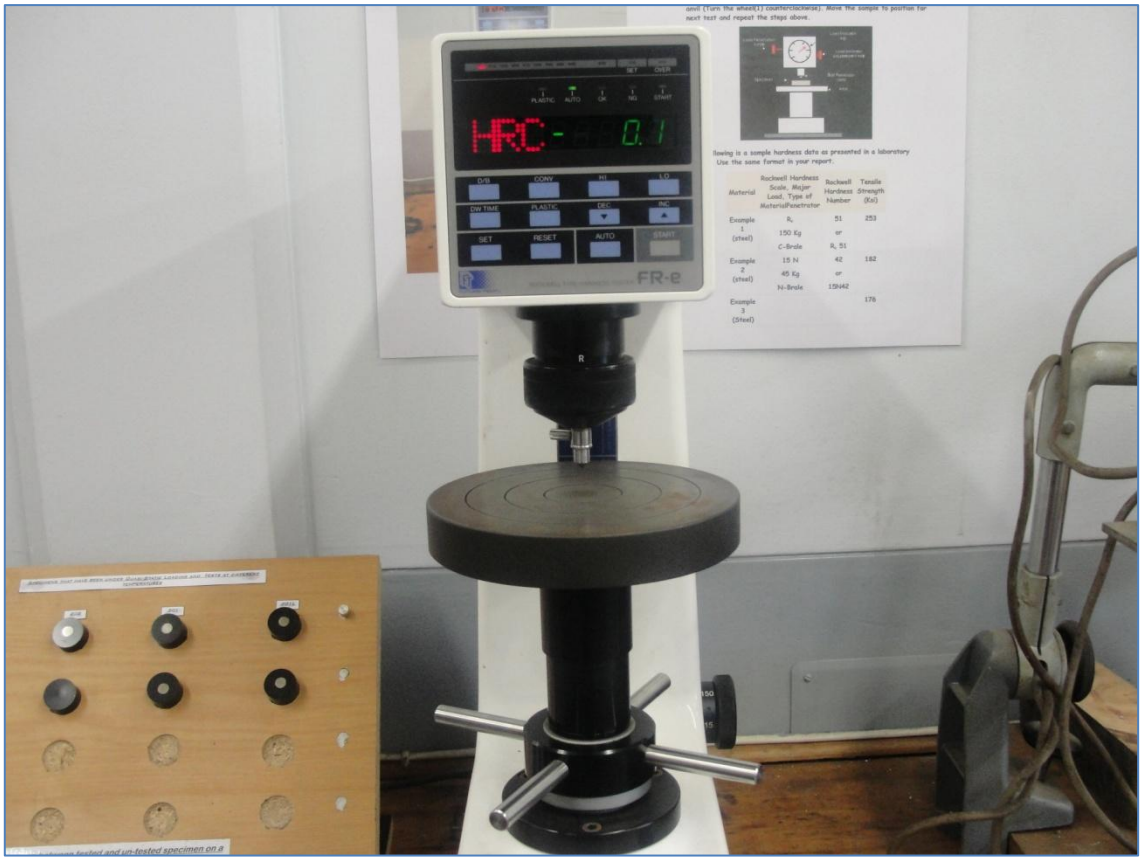

Figure 4.9: Electronic Rockwell Hardness Tester

Mechanical properties of the weld specimen are tested through the Rockwell B hardness test as well as Vickers tester. Hardness is known as a measure of the material's resistance to plastic deformation. The Electronic Rockwell Hardness Tester, shown in figure 4.9 was used for hardness measurement. The prepared specimen is shown in figure 4.10; the marked points illustrate the positions on the specimen where measurements were made. Table 4.3 gives the values of hardness measured in this study.

Figure 4.10: Hardness Test Specimen

The measured values are then compared with the calculated values in table 4.4, and they are found to be in agreement. Apart from the plate-side HAZ, all calculated and measured hardness values are within 10% deviation of each other. The relatively lower measured values also indicate that weld metal and HAZ are tougher than anticipated. The ultimate tensile strength values, that are equivalent to the determined hardness, are also given in the table.

Table 4.3: Measured Hardness Values

Specimen	Plate		Plate HAZ		Weld metal		Pipe HAZ		Pipe	
	HRB	HV	HRB	HV	HRB	HV	HRB	HV	HRB	HV
Specimen	77.1	141	82.1	160	92.1	204	90.5	194	85.3	172
1	80.1	152	91	196	89	188	88.5	186	86.6	178
	82	160	94	213	89.3	188	74.2	135	84.1	168
Specimen	82.5	162	88.3	184	95	217	91.4	197	82.1	160
2	82.5	162	84.8	172	89.4	188	92.5	206	87.4	180
	81.8	160	91.3	196	91.8	204	95	217	80.2	152
Average	81	156	88.5	187	91.1	198	88.7	189	84.3	168
UTS MPa	517		598		641		599		545	

The sections of the specimen that were examined include the weld metal, the HAZ on the plate side, the HAZ on the pipe side and the parent metal. It can be seen from table 4.3 that the parent metal is the least hard of all sections, while the weld metal is the hardest part, followed by the HAZ regions. The microstructure composition of the various regions attests to this, with FZ and HAZ being relatively martensitic structure while the parent metal comprises of mostly pearlite/ferrite microstructure.

4.2.3 Phase Transformation Validation

The last part of the validation experimental work comprises the determination of phase transformation that took place during welding. This is done through microstructure characterisation, which gives insight into the nature of the microstructure of both the FZ and HAZ. The part that was prepared for macrographs above, is used for the purposes of microstructure characterisation. Light Optical Microscopy (LOM) is one of the most commonly used techniques for microstructure characterisation in weld metallurgy. Figure 4.11 shows the advanced Nikon Eclipse MA200 microscope, which was used for this part of experiments.

Figure 4.11: The Nikon MA200 Electronic Microscope

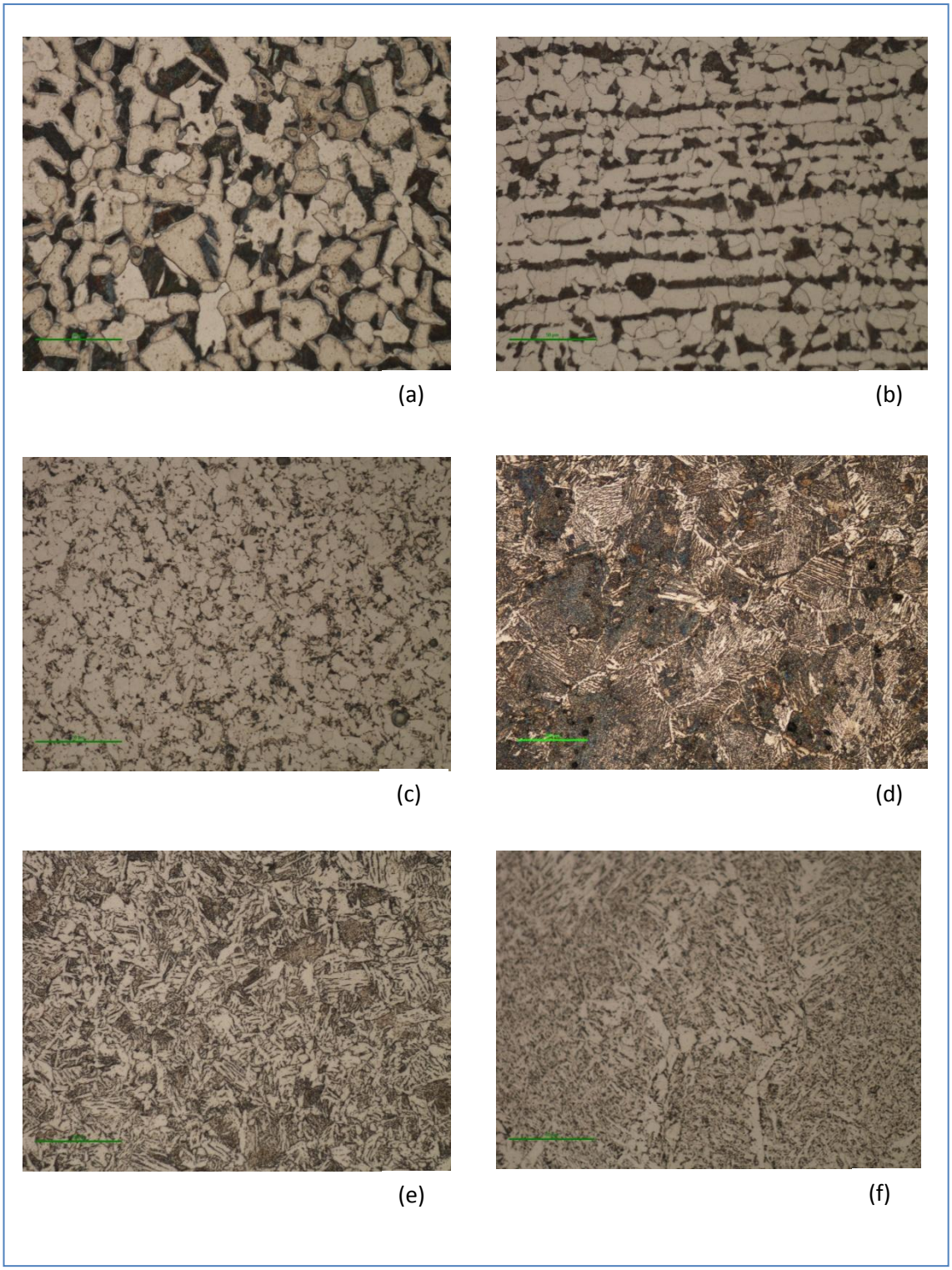

Figure 4.12: The FZ and HAZ Microstructure Characterisation. (a) Pipe Parent Metal; (b) Plate Parent Metal; (c) Weld Metal; (d) HAZ on Pipe Side; (e) CGHAZ on Plate Side; (f) FGHAZ on Plate Side

The results for the macrostructure characterisation are shown in figure 4.12. The parent metals for both the pipe and the plate comprises of pearlite and ferrite. The horizontal lines shown in (b) are the evidence of the cold-rolling process of the ASTM 516 plate material. The weld metal is mainly ferritic with clear traces of martensite. Martensite is more visible in the HAZ regions on both the pipe side and the plate side as shown in (d), (e) and (f). Trapped carbon [martensite] can be seen in the CGHAZ microstructure shown in (e). The rapid cooling at room temperature resulted in the formation of martensite around the FZ and HAZ regions as was expected. It was therefore necessary to incorporate phase transformation effects during the FE modelling, given the evident presence of martensite.

4.3 Empirical Analysis

The empirical analysis for the present study comprises mostly the calculations for maximum hardness in the FZ and HAZ regions of the welded structure. The formulae used are based on experimental studies by Kasuya *et al* (1995). The principle is that maximum hardness depends on the chemical composition of the material and the cooling rate of the weld-piece; and knowledge of these allows for the maximum hardness to be predicted so as to determine the susceptibility to failures such as cold cracking.

4.3.1 Maximum Hardness Calculations

Cold cracking or hydrogen-induced-cracking [HIC] is one of the most significant factors that reduce life expectancy of the welded structure. The main factors that contribute to HIC include microstructure of high hardness, hydrogen content and tensile restraint stresses. The maximum HAZ hardness [often limited to 350 HV for HSLA steels] is generally regarded as an approximate index for susceptibility to cold cracking [Bang *et al*, 2002].

Kasuya *et al* (1995) suggested a formula to work out maximum hardness as follows:

$$HV = \frac{H_M + H_B}{2} - (H_M - H_B).\frac{\arctan(X)}{2.2} \quad (4.1)$$

Where;

H_M is the hardness value where martensite volume fraction reaches 100% in CG HAZ

H_B is the hardness value where martensite volume fraction becomes almost zero per cent in in CG HAZ.

X is defined by: $X = \frac{4.\log(\frac{\tau}{\tau_M})}{\log(\frac{\tau_B}{\tau_M})} - 2$ (4.2)

Where;

τ is the cooling time between 800°C and 500°C [$t_{8/5}$]

τ_M is the cooling time corresponding to H_M

τ_B is the cooling time corresponding to H_B

The four constants [H_M, τ_M, H_B and τ_B] depend on the chemical composition of steel [i.e. weight - %] and are defined as follows:

$$H_M = 884C(1 - 0.3C^2) + 297 \quad (4.3)$$

$$\tau_M = \exp(10.6CE1 - 4.8) \quad (4.5)$$

$$CE1 = C_p + \frac{S_i}{24} + \frac{M_n}{6} + \frac{C_u}{16} + \frac{N_i}{12} + \frac{C_r(1-0.16.\sqrt{C_r})}{8} + \frac{M_o}{4} + \Delta H \quad (4.6)$$

$C_p = C$ for $C \leq 0.3$ and $\frac{C}{6} + 0.25$ for $C > 0.3$

$\Delta H = 0$ for $B \leq 1ppm; 0.03f_N$ for $B = 2ppm; 0.06f_N$ for $B = 3ppm; 0.09f_N$ for $B \geq 4$; where 'B' is the boron content for S $\leq$ 0.016 wt.%

$$f_N = \frac{(0.02-N)}{0.02} \quad (4.7)$$

$$H_B = 145 + 130\tanh(2.65CE2 - 0.69) \quad (4.8)$$

$$CE2 = C + \frac{S_i}{24} + \frac{M_n}{5} + \frac{C_u}{10} + \frac{N_i}{18} + \frac{C_r}{5} + \frac{M_o}{2.5} + \frac{V}{5} + \frac{N_b}{3} \quad (4.9)$$

$$\tau_B = \exp(6.2CE3 + 0.74) \quad (4.10)$$

$$CE3 = C_p + \frac{M_n}{3.6} + \frac{C_u}{20} + \frac{N_i}{9} + \frac{C_r}{5} + \frac{M_o}{4} \quad (4.11)$$

The above equations are used to calculate maximum HAZ hardness from the chemical composition, and calculate cooling time from the thermal analysis. Cold cracking is determined through comparing the calculated maximum HAZ hardness with limiting hardness of 350 HV. The geometry of FZ and HAZ is predicted from the peak temperature distribution. Average peak temperatures of **1316°C** and **954°C** represent CG HAZ and FG HAZ respectively [Bang *et al*, 2002].

The chemical composition of filler metal, plate material and pipe material as given in table 3.2 was used to calculate the maximum hardness of the FZ, the HAZ on the plate side and the HAZ on the pipe side respectively. Energy input per unit length as presented in table 3.3 was utilised for the calculation of cooling rate t_{8-5}. Appendix B provides a graph from where the value of the cooling rate can be read using the heat input value. The average heat input value for the experiments conducted in this study is 0.7 MJ/m, which results to t_{8-5} of 3.2 seconds. The Boron

content is assumed to be 2, thereby giving a value of ΔH of 0.03. The resultant maximum hardness values are given in table 4.3 for all targeted parts of the weld-piece.

Table 4.4: Calculated Hardness Values

Hardness	Fusion Zone	Plate-side HAZ	Pipe-side HAZ
H_M	**376**	**472**	**472**
H_B	**195**	**211**	**192**
HV_{max}	**209**	**243**	**213**

It can be seen from table 4.4 that all maximum hardness values are well below the 350 limit, which mean that the structure is less susceptible of HIC.

Chapter 5

Discussion of Results and Conclusions

The preceding chapters gave a detailed analysis, both numerically and experimentally, of the behaviour of welding-induced residual stress stresses and distortions in SMAW welded pressure vessel nozzle-joints. The numerical results were validated to be within reasonable agreement with the experimental results. This final chapter gives a brief discussion of the findings, conclusions and recommendation of the present study

5.1 Main Findings of the Study

The main findings of the present study can be summarised as follows:

a. The 2D axisymmetric FE model is an effective, cost-effective and time-saving method of thermo-mechanical analysis. The results produced by the model are comparable with results from similar studies performed through 3D FE models.

b. The welding process produces significantly high residual stresses, whose value approaches that of the material yield stress. If such stresses are not effectively treated, they may significantly affect fatigue performance of the welded structure.

c. The produced stresses and distortions are concentrated around the FZ and the HAZ regions. The magnitude of the stresses and distortions rapidly decrease as distance away from weld centre-line increases.

d. The inside surface of the vessel or pipe is under tensile stress, while the external surface is under compressive stress.

e. The microstructure of the FZ and the HAZ comprises a combination of ferrite and martensite. On the other hand, the parent metal is pearlitic/ferritic. Rapid cooling at room temperature [with no preheat] therefore resulted in formation of martensite in the weld metal and HAZ.

f. Hardness tests show that the weld metal and HAZ regions are harder than the parent metal. This is supported by the microstructure characterisation, which shows martensitic structure around the weld zone and HAZ, and peartic/ferritic structure of the parent metal

g. Heat input is the most influential parameter that determines the residual stress distribution during the welding process.

5.2 Mitigation Techniques

A number of welding parameters that are influential in determining the resultant residual stress and distortions were discussed in chapter two above. Identifying such parameters alone is not adequate, hence this section discusses techniques that could be used to mitigate the impact of some of these.

5.2.1 Welding Parameters

Welding Speed and Heat Input: A parametric analysis including three different welding speeds, and with all other factors kept constant, revealed that significantly higher residual stresses are observed – both on the inner and outer surface – at lower welding speeds than higher speeds [Qureshi, 2004]. Such observation can be attributed to the fact that lower welding speeds result in higher heat input per unit volume, and consequently wider FZ and HAZ regions are obtained, thereby causing higher residual stresses. The effect of heat input is the same as that of welding speed. Optimal heat input can therefore be obtained through ensuring optimal values of voltage, current and welding speed for a particular welding procedure.

Welding Sequence: The alternating welding sequence should as far as practically possible be the preferred method over the progressive or continuous welding sequence. The former is implemented through alternating the weld passes [or portions thereof] between various directions or sides of the weld-piece in order to allow more inter-pass cooling time and less heat build-up. The resultant impact is the reduction of residual stress and distortions.

Special welding consumable: After welding, high tensile residual stresses are formed at the weld toe. The magnitude of the tensile stress has been shown to be even higher in high strength carbon steels compared to ordinary mild steel with relatively lower yield strength [Feng, 2005]. In order to prevent stress-induced cracking at the weld toe, compressive stresses have to be introduced to 'neutralise' the tensile stresses. One way of achieving such result is to use a lower-temperature-transformation consumable, which induces compressive residual stresses through the volumetric expansion due to martensitic transformation at lower temperatures. Experiments that were recently performed showed that low-temperature martensitic transformation neutralises the tensile stress from the cooling process and reverses the residual stress direction [Feng, 2005].

Radius : thickness (R/t) Ratio or Wall thickness: Axial stresses increase in the FZ and HAZ as the R/t ratio of the pipe decreases. This can be attributed to the fact that the pipe is stiffer at a lower R/t ratio and there is more constraint at the axial direction. On the other hand, however, the hoop residual stress increases as the R/t ratio increases. Qureshi (2004) studied three wall thicknesses [i.e. 3, 4 and 5mm] to determine impact thereof on residual stress distribution. The study showed that a decrease of about 100 MPa in compressive stress could be achieved by increasing cylinder wall thickness from 3 to 5mm. However, increased wall thickness also results in enhanced stress zone of influence. An optimal R/t ratio or wall thickness, that will balance axial and hoop stresses, as well as stress zone of influence, must therefore be determined for specific cases.

Post-weld heat treatment (PWHT): PWHT comprises the heating of parts [or all] of the welded structure to high temperatures [depending on the material] and holding at such temperature for a predetermined period of time while the stresses are relieved. A rule of thumb is to hold the structure for about one hour for every 25mm thickness. The procedure can be carried out in a furnace or on site using heater blankets, flame torch or similar methods. A number of numerical and experimental studies has been done on PWHT as a form of thermal stress relief [TSR]. It has been shown through such studies that PWHT is an effective method of reducing residual stress, on the surface of the welded structure, to lower levels within the elastic range [Qureshi, 2004]. PWHT has an effect of reducing the magnitude of tensile residual stresses in the FZ and HAZ regions, thereby improving fatigue performance of the joint.

It has been observed that the residual stress in pipe-cylinder welds vary linearly with temperature. Residual stress will decrease by the yield stress ratio [i.e. Yield Stress at T_2 / Yield Stress at T_1, where $T_2 > T_1$] whenever the temperature of the welded structure is uniformly increased. This effectively means that nozzle-vessel joints that are exposed to high operating temperatures experience lower residual stresses than those operating at room temperature. This fact should be considered when predicting the fatigue life of the welded structure.

Mechanical Stress Relieving (MSR)***:*** MSR treatments are carried out to reduce stress field by mechanically loading the welded structure, thereby introducing a new stress distribution. The load is thereafter removed and reduced net residual stresses occur as a result. Some of the widely used MSR treatments include axial pull, application of external pressure and application of internal pressure. In pressure vessel applications, the internal pressure method – which entails the application of hydrostatic pressure on the internal walls of the vessel and nozzles – is widely favoured for its simplicity and effectiveness. Also known as autofrettage, the internal pressure application technique is a process whereby a cylindrical or spherical pressure vessel is subjected to high internal pressure till its walls become partially plastic. The hydrostatic

pressure application has an effect of improving the fatigue life of the vessel through the imposing of favourable compressive stresses to counteract the tensile stresses on the inner surface of the vessel.

5.3 Conclusions

In the present study, numerical methodology based on finite element analysis for the determination of temperature profiles and subsequent welding-induced residual stresses and distortions in SMAW welded pressure vessel nozzle joints of high strength carbon steel are developed and implemented successfully. The results of such numerical analysis are compared with experimental results and found to be within reasonable correlation. A set of conclusions can now therefore be drawn from the above discussion.

Residual Stress and Distortions

The following conclusions are drawn with regards to welding-induced residual stress and distortions:

a. Hoop and axial residual stresses are symmetrically distributed due to the symmetry that exists across the weld line.
b. In the FZ and HAZ regions, high tensile axial stresses, that are close to the yield stress of the material, are present at the inner surface of the nozzle-vessel joint. Similarly, the outer surface experiences high compressive stresses.
c. Residual stress magnitude decreases and changes direction as distance away from weld centre-line increases.
d. In the FZ and HAZ regions, maximum axial and radial deflection occur. As the distance away from weld centre-line increases, axial shrinkage decreases and reaches zero at the restrained end. However, the free end experiences some deflection.

Microstructure of FZ and HAZ

a. The microstructure of the FZ comprises of ferritic/martensitic microstructure.
b. The HAZ metallurgical outlook is dominated by martensitic structure with clear visibility of trapped carbon inside the bcc microstructure

Mechanical Properties

a. The Hardness tests show that the weld metal and HAZ regions are harder than the parent metal. This is supported by the microstructure characterisation, which shows

martensitic structure around the weld zone and HAZ, and peartic/ferritic structure of the parent metal.

Welding Parameters

A detailed review of studies that discussed the influence of welding parameters on residual stress and distortions of welded structures was performed in chapter two above. The following conclusions can be drawn from such discussion:

a. Heat input is the most influential parameter in the creation of welding-induced residual stress and distortions. Increasing the value of heat input [either directly or indirectly] results in enhancement of residual stress fields
b. Pipe wall thickness generally varies inversely with residual stress. Increasing wall thickness results in a decrease of both axial and hoop stresses. However, larger wall thickness also increases the stress zone of influence. It is therefore prudent to determine optimal wall thickness for a specific case.
c. Root-gap opening assists in ensuring weld penetration. However, it also causes axial displacement due to increased lateral shrinkage. Root-gap must therefore just be adequate for weld penetration.
d. Restraints have an influence on axial deformation of circumferentially welded structures. Low restraint produces high axial deformation, and vice versa. The impact of restraints on residual stress magnitude is not significant.
e. The alternating welding sequence is a useful tool of ensuring longer inter-pass cooling time and less heat build-up during welding, which in turn results in reduced residual stress.

Mechanical Stress Relieve (MSR) Treatments

a. Internal pressure application or autofrettage is the most effective MSR treatment method. The applied hydrostatic pressure introduces the compressive stresses on the internal surface of the welded structure, which is already under tensile stress. The compressive stresses neutralise the tensile stresses, thereby causing stress relief.

5.4 Recommendations

The present study has successfully addressed some of the important questions within the subject of pressure vessel fabrication and repairs. It is therefore recommended that the information tabled in the present study be used in industrial applications in order to improve fatigue

performance of nozzle-shell joints in pressure vessels. It is recommended that the provided information is included into the standard operating procedures for pressure vessel fabrication, repairs and preventive maintenance. It is also recommended that the techniques discussed in this study are employed to predict the fatigue life of the pressure vessel structure under specific operating conditions.

The scope of the present study did not extend to the optimisation of the welding process in order to achieve the most optimally performing nozzle-shell joint. Instead the study identified the important weld parameters and suggested ways of mitigating their influence. It is therefore recommended that for further studies, the scope be extended to include the optimisation [possibly through advanced mathematical modelling approaches] of welding parameters in order to achieve an optimal weld joint.

APPENDIX A

CATEGORIES OF RESIDUAL STRESSES AND DISTORTIONS

RESIDUAL STRESS CLASSIFICATION			DISTORTIONS CLASSIFICATION		
Lifespan	**Direction**	**Origin**	**Lifespan**	**Direction**	**Origin**
Temporal [i.e. exists in a specific moment]	Longitudinal [i.e. parallel the welding direction]	Thermal Stress [i.e. caused by non-uniform temperature distribution]	Temporal [i.e. exists in a specific moment]	Longitudinal [i.e. parallel the welding direction]	Caused by non-uniform temperature distribution during welding
Residual [i.e. exists after processing such as welding]	Transversal [i.e. perpendicular to the welding direction]	Phase Transformation Stress [i.e. caused by volumetric changes at high temperature]	Residual [i.e. exists after processing such as welding]	Transversal [i.e. perpendicular to the welding direction]	
		Plastic Deformation Stress [i.e. occurs in areas close to the weld and on the weld itself]		Angular Distortion [i.e. caused by non-uniform temperature distributions in the "through-thickness" direction	
				Rotational Distortion [i.e. angular distortion in the plane of the plate due to thermal expansion or contraction	
				Bending Distortion [i.e. distortion in the plane through the weld line and perpendicular to the plate]	
				Buckling Distortion [i.e. distortion caused by compressive stresses inducing instability on thin plates	

APPENDIX B

Cooling Time vs. Arc Energy for Air and Water-Cooled SMAW Welds for ASTM A517 grade 70 Steel

Source: Johnson (1997)

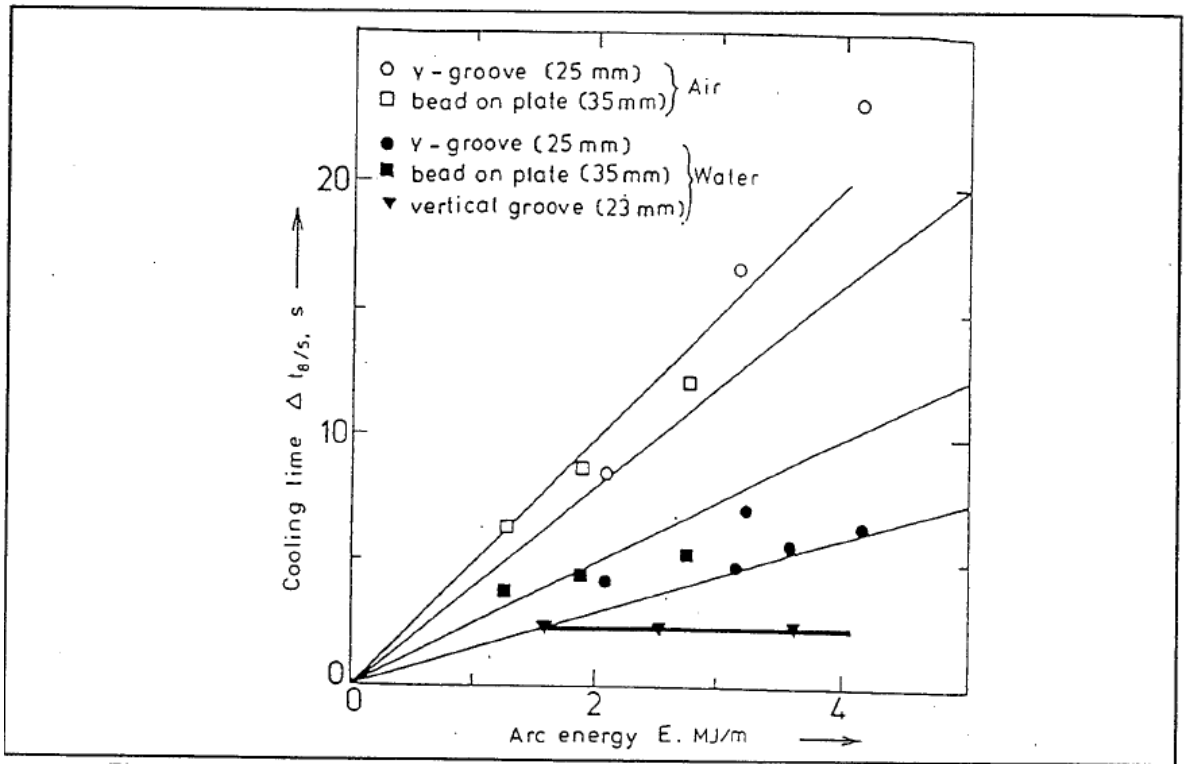

Bibliography

ANCA, A.; CARDONA, A.; RISSO, J.; FACHINOTTI, V.D. (2010). Finite Elements Modelling of Welding Process. Applied Mathematical Modelling - Article in Press, downloaded from www.elsevier.com/locate/apm on 18 November 2010

ARAI, Y.; KIKUCHI, M.; WATANABE, T.; NAKAGAKI, M. (1995): Residual Stress Due to Welding and its Effect on the Assessment of Cracks Near the Weld Interface. International Journal of Pressure Vessel and Piping Vol.63, pp 237-248.

BALASUBRAMANIAN, V.; GUHA, B. (2004). Effect of Welding Processes on Toe-cracking Behaviour of Pressure Vessel Grade Steel. Engineering Failure Analysis, Vol. 11, pp. 575-587

BRUST, F.W.; ZHANG, J.; DONG P.(1997). Pipe and Pressure Vessel Cracking: The Role of Weld-induced Residual Stresses and Creep Damage During Repair. Transactions of the 14th International Conference on Structural Mechanics (SMIRT 14), Lyon, France, August 17-22, 1997.

BANG, I.-W.; SON, Y.-P.; OH, K.H.; KIM, Y.-P.; KIM, W.-S. (2002). Numerical Simulation of Sleeve Repair Welding of In-service Gas Pipelines. Welding Journal, Dec. 2002, pp. 273-282

DENG, D. (2009). FEM Prediction of Welding Residual Stress and Distortion in Carbon Steel Considering Phase Transformation Effects. Materials and Design. Vol.30, pp. 359-366.

DENG, D.; MURAKAWA, H. (2006). Numerical Simulation of Temperature Field and Residual Stress in Multi-pass Welds in Stainless Steel Pipe and Comparison with Experimental Measurements. Computational Material Science, Vol.37, pp. 269-277

DENG, D.; MURAKAWA, H. (2006b). Prediction of Welding Residual Stress in Multi-pass Butt-welded Modified 9 Cr-1Mo Steel Pipe Considering Phase Transformation Effects. Computational
Material Science, Vol. 37, pp.209-219

DENG, D.; MURAKAWA, H. (2008). Finite Analysis of Temperature field, microstructure and Residual Stress in milti-pass butt-welded 2.25 Cr-1Mo Steel Pipes.
Computational Materials Science, Vol. 43, pp 681-695.

DILL, F. (1997). Model for Estimation of Thermal History Produced by a Single Pass Underwater Wet Weld. MSc.Eng. Thesis. Naval Postgraduate School, Monterey, California.

DONG, P.; HONG, J.K.; BOUCHARD, P.J. (2005). Analysis of Residual Stresses at Weld Repairs. International Journal of Pressure Vessels and Piping, Vol.82,pp. 258-269.

ELMER, J.W.; PALMER, T.A.; ZHANG, W.; WOOD, B. DEBROY, T. (2003). Kinetic Modelling of Phase Transformation Occuring in the HAZ of C-Mn Steel Welds Based on Direct Observation. Acta Materials, Vol.51, pp. 3333-3349

FACHINOTTI, V.D.; CARDONA, A. (2008). Semi-Analytical Solution of the Thermal Field Induced by a Moving Double-Ellipsoidal Welding Heat Source in a Semi-Infinite Body. Asociación Argentina de Mecánica Computacional, Vol. XXVII, pp. 1519-1530

FENG, Z. (2005). Processes and Mechanisms of Welding Residual Stress and Distortion. Woodhead Publishing in Materials, Cambrige England.

FORD, F.P.; SCOTT, P.M. (2008). Environmentally Assisted Degradation of Carbon and Low Alloy Steels in Water-Cooled Nuclear Reactors. Advanced Nuclear Technology International. Special Report

GANNON, L.; LIU, Y.; PEGG, N.; SMITH, M. (2010). Effect of Welding Sequence on Residual Stress and Distortion in Flat Bar Stiffened Plates. Marine Structures, Vol.23, pp. 385 - 404

GERY, D.; LONG, H.; MAROPOULOS, P. (20050. Effects of Welding Speed, Energy Input and Heat Source Distribution on Temperature Variations in Butt-Joint Welding. Journal of Materials Processing Technology, Vol. 167, pp. 393-401

JAHROMI, B.H.; FARRAHI, G.H.; MALEKI, M.; NAYEB-HASHEMI, H.; VAZIRI, A. (2009). Residual Stresses in Autofrettaged Vessel Made of Functionally Graded Material. Engineering Structures, Vol.31, pp. 2930-2935

KARLSSON, L (2005). Residual Stresses Due to Welding of a Nozzle to a Pressure Vessel. Master's Dissertation, Division of Solid Mechanics, Lund University, Sweden.

KASUYA, T.; YURIOKA, N.; OKUMURA, M. (1995). Methods for Predicting Maximum Hardness of HAZ and Selecting Necessary Preheat Temperature for Steel Welding. Nippon Steel Technical Report, 65(4), pp. 7-14

KEEHAN, E. (2004). Effect of Microstructure on Mechanical Properties of High Strength Steel Weld Metals. A PhD Thesis, Department of Experimental Physics, Chalmers University of Technology and Goteborg University, Sweden.

KISIOGLU Y. (2005). Effects of Weld Zone Properties on Burst Pressures and Failure Locations. Turkish Journal of Engineering and Environmental Science, Vol. 29, pp 21-28.

KOH, S-K. (2000). Fatigue Analysis of Autofrettaged Pressure Vessels with Radial Holes. International Journal of Fatigue, Vol.22, pp. 717-726

KOU, S. (2003). Welding Metallurgy, 2nd Edition. John Wiley and Sons, USA

LEE, C-H.; CHANG, K-H (2008). Three Dimensional Finite Element Simulation of Residual Stresses in Circumferential Welds of Steel Pipe Including Pipe Diameter Effects. Materials Science and Engineering, A 487, pp. 210-218.

LEE, C-H.; CHANG, K-H. (2009). Finite Element Simulation of the Residual Stresses in High Strength Carbon Steel Butt Weld, Incorporating Solid-State Phase Transformation. Computational Material Science, Vol.46, pp.1014-1022

LEE, S-I.; KOH, S-K. (2002): Residual Stress Effects on the Fatigue Life of an Externally Grooved Thick—walled Pressure Vessel. International Journal of Pressure Vessels and Piping, Vol. 79, pp. 119-126.

LEGGATT, R.H. (2008). Residual Stress in Welded Structures. International Journal of Pressure Vessels and Piping, Vol. 85, pp. 144-151.

LINDGREN, L.-E. (2006). Numerical Modelling of Welding. Computer Methods in Applied Mechanics and Engineering, Vol.195, pp. 6710-6736

LINGAMANAIK, S.N.; CHEN, B.K. (2011). Thermo-mechanical Modelling of Resdiual Stresses Induced by Martensitic Phase Transformation and Cooling During Quenching of Railway Wheels. Journal of Materials Processing Technology, Vol. 211, pp. 1547-1552

MALEKI, M; FARRAHI,G.H; HAGHPANAH JAHROMI, B.; HOSSEINIAN,E. (2010). Residual Stress Analysis of Autofrettaged Thick-walled Spherical Pressure Vessel. International Journal of Pressure Vessels and Piping, Vol. 87, pp. 396-401

MALIK, M.A.; QURESHI, M.E.; DAR, N.U. (2007). Numerical Simulation of Arc Welding Investigation of Various Process and Heat Source Parameters. Failure of Engineering and Structures, Vol.30, pp. 127-142

MORAITIS, G.A.; LABEAS, G.N. (2009). Prediction of Residual Stresses and Distortions due to Laser Beam Welding of Butt Joints in Pressure Vessels. International Journal of Pressure Vessel and Piping, Vol. 86, pp. 133-142

NONAKA, I.; ITO, T.; OHTSUKI, S.; YAKAGI, Y. (2001). Performance of Repair Welds on Aged 2.25_Cr-1Mo Boiler Header Welds. International Journal of Pressure Vessels and Piping, Vol. 78, pp. 807-811.

OZCATALBAS, Y.; VURAL, H.I. (2009). Determination of Optimal Welding Sequence and Distortion Forces in Steel Lattice Beams. Journal of Material Processing Technology, Vol.209, pp. 599 - 604

PILIPENKO, A. (2001). Computer Simulation of Residual Stress and Distortion of Thick Plates in Multi-Electrode Submerged Arc Welding. Their Mitigation Techniques. A PhD Dissertation, Department of Machine Design and Materials Technology, Norwegian University of Science and Technology, Trondheim, Norway.

QURESHI, M.E. (2004).Analysis of Residual Stresses and Distortions in Cirfumferentially Welded Thin-walled Cylinders. A PhD Thesis. National University of Science and Technology, Pakistan

RYBICKI, E.F; SCHUESER, D.W.; STONESIFER, R.B.; GROOM, J.J.; MISHLER, H.W. (1977). A Finite Element Model for Residual Stress. ASME Winter Annual Meeting, Nov 1977, Atlanta, Ga.

SATTARI-FAR, T.; JAVADI, Y. (2008). Influence of Welding Sequence on Welding Distortions on Pipes. International Journal of Pressure Vessels and Piping, Vol. 85, pp. 265 - 274

SIDDIQUE, M. (2005). Experimental and Finite Element Investigation of Residual Stresses and Distortions in Welded Pipe-flange Joints. A PhD thesis, Ghulam Ishaq Khan Institute of Engineering Sciences and Technology, Pakistan

SMITH, C.; PISTORIUS, P.G.H.; WANNENBURG, J. (1997). The Effect of a Long Post Weld Heat Treatment on the Integrity of a Welded Joint in Pressure Vessel Steel. International Journal for Pressure Vessels and Piping, Vol. 70, pp. 183-195

STERJOVSKI, Z. (2003). Investigation of Post Weld Heat Treatment of Quenched and Tempered Pressure Vessel Steel. A PhD Thesis, University of Wollongong, Australia

STERJOVSKI, Z.; DUNNE, D.P.; AMBROSE, S. (2004). Evaluation of Cross-weld Properties of Quenched and Tempered Pressure Vessel Steel Before and After PWHT. International Journal of Pressure Vessels and Piping, Vol.81, pp. 465-470

TOTTEN, G.; HOWES, M.; INOUE, T. (2002). Handbook of Residual Stress and Deformation of Steel. ASM International, USA

TENG, T-L.; CHANG, P-H.; KO, H-C. (2000). Finite Element Analysis of Circular Patch Welds. International Journal of Pressure Vessels and Piping, Vol.77, pp. 643-650

TENG, T-L.; CHANG, P-H.; TSENG, W-C. (2003). Effect of Welding Sequence on Residual Stresses. Computers and Structures, Vol. 81, pp. 273-286.

WANG, S.; GOLDAK, J.; ZHOU, J.; TCHERNOV, S.; DOWNEY, D. (2009). Simulation on the Thermal Cycle of a Welding Process by Space-Time Convection Diffusion Finite Element Analysis. International Journal of Thermal Sciences, vol.48, pp.936-947

www.residualstress.org, accessed on 03 August 2010, 15h31 SA time

YAGHI, A.; BECKER, A. (2004). State of the Art Review: Weld Simulation Using Finite Element Methods. Publication of the University of Nolfingham, UK

ZARZOUR, J.F.; KONKOL, P.J.; DONG, H. (1996). Stress-Strain Characteristics of the Heat Affected Zone in an HY-100 Weldment as Determined by Microindentation Testing. Materials Characterisation, Vol. 37, pp. 195-209

ZHU, L.; TAO, X.Y.; CENGDIAN, L. (1998). Fatigue Strength and Crack Propagation Life of In-service High Pressure Tubular Reactor Under Residual Stress. International Journal of Pressure Vessels and Piping, Vol. 75, pp. 871-877